β1- and β3-integrins display differential nano-dynamic organizations inside focal adhesions

Olivier Rossier[1,2], Vivien Octeau[3], Jean-Baptiste Sibarita[1,2], Cécile Leduc[3], Béatrice Tessier[1,2], Deepak Nair[1,2], Volker Gatterdam[4], Olivier Destaing[5], Corinne Albiges-Rizo[5], Robert Tampé[4], Laurent Cognet[3], Daniel Choquet[1,2], Brahim Lounis[3], and Grégory Giannone[1,2†]

[1]Univ. Bordeaux, Interdisciplinary Institute for Neuroscience, UMR 5297, F-33000 Bordeaux, France
[2]CNRS, Interdisciplinary Institute for Neuroscience, UMR 5297, F-33000 Bordeaux, France
[3]LP2N, Université de Bordeaux, Institut d'Optique Graduate School and CNRS, 351 cours de la libération, 33405 Talence, France
[4]Institute of Biochemistry, Biocenter, Goethe University Frankfurt, Max-von-Laue Str. 9, D-60438 Frankfurt a.M., Germany
[5]Institut Albert Bonniot, Université Joseph Fourier; INSERM U823; CNRS ERL 3148 Grenoble, France

[†]Corresponding author

Key Words: integrins, adhesion sites, single molecule/protein tracking, super-resolution microscopy

Abbreviations:
D: diffusion coefficient
FAs: focal adhesions
F-actin: filamentous actin
FN: fibronectin
FRAP: fluorescent recovery after photobleaching
MEFs: mouse embryonic fibroblasts
sptPALM: photoactivation localization microscopy
r_{conf}: confinement radius
SMT: single molecule tracking
spt: single protein tracking
STED: stimulated emission depletion
TIRF: total internal reflection fluorescence
TM: transmembrane protein
TrisNTA: Ni^{2+} tris-nitrilotriacetic acid

Introduction

In focal adhesions (FAs), adhesion and force transmitted by integrins to extracellular matrices are crucial for cell motility, proliferation and differentiation[1,2]. Different classes of αβ-integrins binding to fibronectin (FN) perform distinct functions[3-5] and are simultaneously present in FAs. Although, the static nanoscale organization of FAs was recently described[6], explaining how the individual dynamics of specific integrins control biochemical and biomechanical events in FAs is still elusive. By combining super-resolution imaging and single protein tracking we show that β3- and β1-integrins act as distinct adhesion units displaying specific dynamics and organizations within FAs. Integrins reside in FAs through cycles of free-diffusion and immobilization, supporting that integrins are not constantly active inside FAs. Integrin activation promotes immobilization, while inhibition of FN or F-actin binding increases free-diffusion, suggesting that full integrin immobilization requires simultaneous F-actin and FN connections. β3-integrins immobilization zones are more concentrated within FAs compared to β1-integrins. While β3-integrins immobilization zones are stationary in FAs, immobilization zones for β1-integrins display rearward movements. Using chimeric β1-β3-integrins, we demonstrate that these differences are determined by binding to extracellular FN. Thus, differential transmission of F-actin motion to FN within FA occurs through specific integrins. This dynamic nano-partitioning of β-integrins within FAs could control local forces and signaling necessary for distinct cellular functions such as migration and extracellular matrices remodeling.

Unraveling integrins dynamic organization within FAs is a key step towards a complete understanding of biochemical and biomechanical events controlling FAs architecture. In mature FAs both αvβ3 and α5β1 integrins bind to FN, a major component of the extracellular matrix. Outside FAs, on dorsal surface of fibroblasts, both integrins are freely diffusing when unbound and undergo rearward actin-driven motion after binding to FN[7,8]. This demonstrates that integrin movements are controlled by connection to FN and actin binding proteins (ABP). Yet inside FAs, recording the pristine individual trajectories of integrins has remained challenging because such structures are crowded and confined preventing the use of large probes. Nevertheless, previous ensemble measurements[9-11] suggested that integrins are the most stable components in FAs.

To investigate whether integrin movements differ outside versus inside FAs, we applied super-resolution microscopy to characterize integrins distributions and displacements at a resolution well below the diffraction limit. We first focused on β3-integrin in mouse embryonic fibroblasts (MEFs), using live-cell photoactivation localization microscopy[12] coupled to single protein tracking (sptPALM)[13]. MEFs were spread on FN and co-transfected with GFP-paxillin, as a FAs reporter, and wild type β3-integrin fused to an intracellular mEOS2, a photo-switchable protein (β3-WT). Binary masks of FAs were generated using GFP-paxillin fluorescent signal. Using total internal reflection fluorescence microscopy (TIRF), numerous sparse β3-WT were continuously activated, localized and bleached. We reconstructed thousands β3-WT trajectories outside and inside FAs (Fig. 1a). For trajectories lasting at least 400 ms (20 points≤, 8% of the trajectories), we computed the mean square displacement (MSD), which reflects the diffusion properties of a molecule. Variation of the MSD over time was used to sort trajectories according to their diffusion modes (immobile, confined, free-diffusive) (Fig. 1b,e), extract diffusion coefficients (D) and confinement radius (r_{conf}) (Fig. 1f-j, Supplementary Table S1, see Methods). The differential motion of β3-WT inside versus outside FAs was striking as seen by the strong redistribution of D towards faster diffusion outside FAs (Fig. 1f,g). Within the spatial resolution of our experimental setup ($2.3\sigma_{xy}$ ~50 nm, see methods), we found that β3-integrins were mainly immobile in FAs (69±2%, Fig. 1e), the remaining ones displaying either confined diffusion (14±1%; r_{conf}=119±1 nm, Fig. 1h; D=0.043±0.001 $\mu m^2.s^{-1}$, Fig. 1i) or free-diffusion (17±1%; D=0.076±0.001 $\mu m^2.s^{-1}$, Fig. 1j). In contrast, outside FAs, β3-integrins immobilization decreased (46±3%), the fraction of free-diffusive integrins increased (39±3%) and free-

diffusion was faster (D=0.289±0.003 $\mu m^2.s^{-1}$). Furthermore, confined integrins displayed increased r_{conf} and D outside FAs (r_{conf}=236±3 nm; D=0.189±5 $\mu m^2.s^{-1}$). Therefore, in FAs immobilizations were more frequent, areas of confinements were smaller and free-diffusions were slower. To ensure that these diffusion properties were specific to integrins, we analyzed trajectories of mEOS2 fused to the trans-membrane domain of the PDGF receptor (mEOS2-TM) or anchored to inner leaflet lipids (CAAX-mEOS2) (Fig. 1c,d). The results demonstrated that frequent immobilizations and slower free-diffusions of β3-WT were triggered by integrin specific interactions in FAs, rather than by the higher protein density present in FAs (Fig. 1e-j). Therefore, integrin binding partners in FAs increase the probability of β3-integrin arrest and could contribute to FAs formation and stability through a diffusion/trapping mechanism.

To determine whether the level of integrin activation controls β3-integrin immobilization in FAs, we used Mn^{2+} stimulation or a glycan edge point mutation stabilizing the active conformation of β3-integrin (β3-N305T)[9,14] (Fig. 2a). Stimulated β3-integrins exhibited nearly the same dynamics as β3-WT in FAs, but outside FAs immobilization increased, r_{conf} and free-diffusion decreased dramatically close to values measured for β3-WT inside FAs (Fig. 2b-e, Supplementary Fig. S1). These results demonstrated that promoting integrin activation outside FAs bypassed signals inducing immobilization in FAs. This support that integrin immobilization and slower free-diffusion triggered outside FAs are the consequence of increased integrin binding to the extracellular matrix, which is commonly defined as integrin activation[15,16].

Next we examined how interactions with FN and F-actin respectively regulate integrin motion. We used known integrin point mutations, β3-D119Y which prevents binding to the RGD sequence of FN[9], and β3-Y747A which inhibits connection to critical actin binding proteins (ABP) such as filamin, tensin and talin[9,16-18] and prevents β3-integrin activation[15]. Inhibiting FN or ABP binding decreased the fraction of immobilization and increased r_{conf} inside FAs (Fig. 2f-j, Supplementary Fig. S1). These mutants also showed faster D inside FAs indicating that transient interactions with FN and ABP slowdown integrin motion in FAs, rather than steric hindrance due to molecular crowding. Dynamics of WT and mutant β3-integrins were not affected by the probes used to localize FAs (GFP-paxillin or GFP-VASP) (Supplementary Fig. S2, Supplementary Table S2), or by the presence of endogenous β3-integrins, as indicated by experiments performed in β3-integrin$^{-/-}$ MEFs (Supplementary Fig.

S2, Supplementary Table S3). Thus, conditions promoting integrin activation triggers immobilization, while preventing FN or ABP binding increases free-diffusion.

We next investigated if β3-integrin immobilization was preferentially triggered by FN or ABP binding. Inside FAs, when preventing binding to ABP compared to FN, we systematically measured stronger reduction of the immobilized fraction, larger r_{conf}, and faster free-diffusion. This was confirmed both when GFP-paxillin or GFP-VASP were used as FAs reporter, or in β3-integrin$^{-/-}$ MEFs (Fig. 2, Supplementary Fig. S1,S2). Despite binding of filamin, tensin and talin to the same NPxY motif on integrin tails, the most compelling evidences for inside-out integrin activation involve talin[18-20]. Thus talin is the best ABP candidate to induce integrins immobilizations, which is consistent with its critical role during FAs initiation[21,22]. Therefore, although FN and ABP binding are required for efficient integrin immobilization, our results suggest that ABP binding triggers immobilization more efficiently than FN binding.

To test if binding to FN and ABP also control integrins immobilization time, we used sptPALM experiments to assess the duration of immobilization zones. Immobilization zones were identified by locations where repetitive mEOS2 fluorescence were detected (Fig. 3a, Supplementary Fig. S3, see methods)[23]. We thus estimated the durations of these immobilization zones and compared them for β3-integrin WT and mutants (Fig. 3a-c). By comparing immobilization duration inside and outside FAs for β3-WT we found that immobilization were longer inside FAs, and were shortened by loss of F-actin and FN interactions (Fig. 3c). Kymographs generated from sptPALM super-resolution time-lapses[23] clearly illustrate those differences (Fig. 3a,b). Immobilization durations for β3-D119Y, β3-Y747A were as short inside as outside FAs, while for β3-N305T the durations were increased compared to β3-WT outside FAs. As expected, the duration of immobilization zones for CAAX were short both inside and outside FAs. As a control, the duration measured for β3-WT in fixed cells are longer than in live cells, and well above conditions which shorten the duration of integrin immobilizations. Taken together, these results support that integrin binding to FN or ABP alone does not lead to a full long-lived integrin immobilization, condition achieved only when simultaneous tripartite interaction with FN and APB occurs. Condition often fulfilled in FAs, were ABP including talin are more concentrated.

To demonstrate that β3-integrins switch reversibly between immobilization and free-diffusion within the same FA, we obtained longer trajectories with single molecule tracking (SMT) using photostable ATTO647N dyes (Fig. 3d,e). Extracellular labeling of single 6His-β3-integrins carrying a poly-histidine tag was achieved with ATTO647N/Ni^{2+} tris-nitrilotriacetic acid (TrisNTA), a small (2 nm) and monovalent probe (Supplementary Fig. S4)[24,25]. Using this method, the motions of β3-integrin WT with or without Mn^{2+} stimulation, and of β3-integrins mutants (N305T, D119Y, Y747A) were analyzed inside and outside FAs. We analyzed the degree of molecule mobility by measuring the molecule displacement steps inside and outside FAs. All the major findings obtained by sptPALM were confirmed including, increased immobilization inside FAs and upon integrin activation, decreased immobilization of integrins unable to bind FN or ABP, and higher ABP-dependence on immobilization fraction (Supplementary Fig. S5). Furthermore, long trajectories (>10 s) demonstrated that β3-integrins switch from fast free-diffusion outside FA, to slow free-diffusion and immobilization when entering a FA (Fig. 3d, Supplementary Movie S1). Moreover, β3-integrins exhibited successive immobilizations in the same FA (Fig. 3e). In the current view, integrin biochemical and mechanical signaling are based on the assumption of long-lived integrin interactions with their surroundings. Yet, repeated trappings of integrins seen as cycles of slow free-diffusion and immobilization within a FA support that integrins are not constantly activated in FAs, and not as stable as inferred from previous measurements[9-11].

Different classes of αβ-integrins have been associated with specific properties that serve specific functions[3-5,26]. Former studies[6,9,11] focused on the dynamic and organization of αv- and β3- integrins in FAs. Thus, paradigms of integrin engagement to the extracellular matrix and F-actin are generally built on a homogeneous integrin population in FAs[1,27]. To determine whether β1- and β3-subunits exhibit specific dynamics inside FAs, we performed sptPALM using β1-integrin-mEOS (β1-WT) (Fig. 4a). Like β3-WT, β1-WT immobilization was enhanced inside FAs. Surprisingly, the diffusion parameters measured for β1-WT inside and outside FAs were almost identical to β3-WT (Fig. 4b-e, Supplementary Fig. S6). We then tested whether interactions with FN or ABP regulate β1-WT immobilization. Like αvβ3 integrin, α5β1 integrin binds the RGD sequence of FN[28], and intracellular filamin, tensin and talin[20]. We generated point mutations in β1-integrin corresponding to the ones used for β3-integrin: mutation of β1-D130 prevents binding to the RGD sequence of FN[29] and β1-Y783A

inhibits ABP binding[30] and consequently β1-integrin activation[15]. Like for β3-integrin, ABP binding critically controls β1-integrin immobilization, confinement and free-diffusion, as shown by the behavior of β1-Y783A (Fig. 4b-e, Supplementary Fig. S6). However, in contrast to β3-D119Y integrin, β1-D130Y does not affect β1-integrin immobilization in FAs. Both αvβ3 and α5β1 integrins bind the RGD sequence of FN, but only α5β1 binds the FN synergy site (PHSRN)[29]. Therefore our results suggest that binding of β1-integrin to the FN synergy site might be sufficient to induce immobilization of β1-integrin in mature FAs.

To test whether a specific nanoscale organization of β-subunits exists inside FAs, we examined β1- and β3-integrins immobilization zones and compared their durations and organization. Immobilization durations for β1-WT were longer inside than outside FAs, were shortened when ABP binding was suppressed, but less affected by loss of RGD binding (Supplementary Fig. S6). Thus like the fraction of β1-WT immobilization, the duration of immobilization seems to depend on the FN synergy site. More strikingly, the nano-scale organizations of β3- and β1-integrins were different within FAs as demonstrated by sptPALM super-resolved images. The density of immobilization for β1-integrins was twice lower than for β3-integrins (Fig. 4g,h), as measured by the ratio of inside versus outside detections (Fig. 4f). This distinct organization of β3- and β1-integrins inside FAs were further confirmed using Stimulated Emission Depletion microscopy (STED)[31], an alternative nanoscopic imaging approach (Supplementary Fig. S7).

To trigger cell motility, forces generated by F-actin must be physically transmitted from integrins to FN. One model describing this process is the molecular clutch[27], by which a modular interface of adaptor proteins, including talin, mediates a dynamic mechanical coupling of the F-actin flow to integrins[11]. We thus tested if β-integrins inside FAs exhibited or not rearward actin-driven motion. We measured the slow motion of β1- and β3-integrins immobilization zones from sptPALM super-resolution time-lapses[23] (Fig. 5). Oddly, despite their connection to F-actin through ABP, most β3-integrins were not moving rearward (Fig. 5a,b,e). On the contrary, 40 % of β1-integrin in FAs were moving rearward with rates corresponding to the speed of F-actin within FAs (~4 nm/s)[11] (Fig. 5c,d,e). Thus, specific classes of αβ-integrin will transmit differentially F-actin motion to FN, suggesting that integrin-specific clutch module might exist within FAs.

β3- and β1-integrin cytoplasmic tails bind common[20,32] and specific[33,34] intracellular partner. To differentiate whether extracellular or intracellular domains of β1- and β3-integrins are responsible for specific organization and coupling to F-actin motion, we used chimeric integrins. Extracellular β1-integrin domain was fused to β3-integrin transmembrane and cytoplasmic domains (β1extβ3int) and inversely for β3extβ1int. We performed sptPALM experiments using those chimeras, and found that β1extβ3int behaved like β1-integrin whereas β3extβ1int like β3-integrin. This was confirmed for the short term dynamics measured by sptPALM (Fig. 4d,e, Supplementary Fig. S6), the density of immobilization zones (Fig. 4f) and the rearward motion (Fig. 5f). These results suggest that the extracellular domain of integrins determines the density of integrin immobilization in FAs and how F-actin motion are transmitted to FN.

The direct visualization of integrin motion demonstrated that β3-integrins are immobile and more concentrated in mature FAs. This implies, that F-actin internal forces never reach the level required to displace FN-bound β3-integrins, suggesting that the clutch module associate transiently with β3-integrins. However, during this association, a transient rise in tension, building on immobile β3-integrins, could induce talin stretching and subsequent mechanical reinforcement of F-actin connection[5,21] through vinculin recruitment[35]. This remains true until the weakest link in the integrin/talin/F-actin linkage breaks. After this rupture, β3-integrin still bound to immobile FN could associate again with F-actin or diffuse away to find another anchoring point. On the contrary, β1-integrins move rearward at the speed of F-actin flow. We propose that this motion of β1-integrin within FAs reflect β1-integrins bound to the synergy site of FN. Indeed, binding to the FN synergy site is a major difference between β1- and β3-integrin when binding to FN[29,36]. Thus experiments using chimeric integrins, demonstrating that extracellular domains determine the specific behavior of β-integrins inside FAs, implicate the FN synergy site. Binding to the FN synergy site confers to α5β1-integrin higher adhesion strength[5], but also extracellular mechanical activation[28] possibly driven by a catch bond between α5β1-integrin and FN[37]. Moreover, it has been shown that under FN stretching, the synergy site could be exposed and the RGD site buried, constituting a mechanosensitive control of ligand recognition[28,36]. Therefore, α5β1-integrin can not only sustain higher F-actin forces permitting stretching and unfolding of FN[38], but also could specifically bind to stretched FN. We thus propose that the rearward motion of α5β1-integrins in FAs reflects the preferential binding to a subpopulation of FN, i.e.

stretched or stretchable FN. Since talin unfolding requires level of forces lower than for FN unfolding[35,36], the interface between α5β1-integrins and F-actin should accommodate the load sufficient to stretch FN. This suggests that different clutch modules having distinct mechanical properties are associated with specific integrins. We propose that a slipping interface exist between F-actin and immobile αvβ3-integrins, while the interface between α5β1-integrins and F-actin could accommodate a load used to stretch and remodel FN. This model is consistent with the localization of α5β1 integrin both in FAs and in fibrillar adhesions and its major role in FN fibrillogenesis, as compared to αvβ3 integrin which is only confined to FAs[3,26].

We unravel a nano-partitioning within FAs which defines the precise location and duration of β-integrin-specific biochemical and mechanical signals. We show that this organization is remodeled in less than a hundred seconds through cycles of integrin free-diffusion and immobilization. These cycles permit integrin to probe sequentially for missing binding partners, enabling the progressive building of a tripartite connection between FN/integrin/talin. This more dynamic view of FN/integrin/ABP connection implies to reconsider integrin biochemical and mechanical signaling, such as reinforcement of integrin/F-actin linkages[7], as transient processes constantly relocating within FAs. Our work suggests that the lifecycle of adhesion sites is regulated by the fast remodeling of an integrin mosaic on which intracellular scaffolds and signaling proteins act.

Methods

Cell culture

Immortalized MEFs and β3-integrin$^{-/-}$ MEFs (generously provided by Dr. Richard Hynes (Massachusetts Institute of Technology, Cambridge, MA)) were cultured in DMEM (Gibco) with 10% FBS (v/v). Transient transfections of plasmids encoding the various constructs were performed 1 day before experiments either by using Fugene 6 (Roche, Basel, Switzerland) or by electroporation using a Nucleofector (Lonza, Basel, Switzerland) according to the manufacturer's protocol (MEF-1 solution and program T-20). On the day of the experiments, cells were detached with trypsin/EDTA (0.05% for 2 min), the trypsin inactivated with 10% (v/v) FBS DMEM, the cells washed and suspended in serum free condition in Ringer (in mM: 150 NaCl, 5 KCl, 2 $CaCl_2$, 2 $MgCl_2$, 10 HEPES, 11 Glucose, pH 7.4), and incubated for 30 min before plating on human FN (Roche) glass surface. Experiments were performed 3-5 hours after cell plating.

Antibodies and DNA constructs

ATTO647N dye-conjugated goat secondary antibody against rat IgG (used at 1:200) was obtained from Enzo Life Sciences (Farmingdale, NY, USA). Mouse monoclonal antibody against human αvβ3-integrin (clone LM609; used at 1:100) was purchased from Millipore (Billerica, MA, USA). Rat monoclonal antibody against mouse β1-integrin (clone 9EG7; used at 1:100) was purchased from BD Pharmingen (Franklin Lakes, NJ, USA).

Plasmid pFB-Neo-human β1-integrin-GFP is the generous gift of Martin Humphries (University of Manchester, Manchester, UK). For the mEOS2-tagged human β1-integrin construct, mEOS2 sequence was PCR-amplified and used to replace GFP of pFB-Neo-human β1-integrin -GFP to generate an in-frame C-terminal fusion (as described in ref. [39]). Human β3-integrin-GFP[40], was generously provided by Nelly Kieffer (CNRS/CRP, Luxembourg). Human 6His-β3-integrin-GFP was obtained from the previous one by domain swapping using the QuickChange® II XL Site-Directed Mutagenesis kit (Stratagene) to introduce 6His tag and glycine linker in the N-terminus. For the human 6His-β3-integrin, a PCR of the end of the β3-integrin was done to replace the PstI / BsrGI fragment of the human 6His-β3-integrin-GFP in order to remove the GFP. For the human 6His-β3-integrin-mEOS2, a PCR of mEOS2 was done on pRSETa-mEOS2 (Addgene) to replace the GFP from human 6His-β3-integrin-GFP at the AgeI / BsrGI sites. All the β3-integrin and β1-integrin mutants were generated by site-directed mutagenesis using the QuickChange® II XL Site-Directed Mutagenesis kit (Stratagene). PCR were performed on 6His-β3-integrin, 6His-β3-integrin-mEOS2 and β1-integrin-mEOS2. β3extβ1int chimeric integrin (β3-integrin extracellular domain fused to β1-integrin transmembrane and cytoplasmic domains) fused to mEOS2 was generated by replacing the GFP of the β3extβ1int chimeric[9] by the mEOS2 sequence. For β1extβ3int chimeric integrin (β1-integrin extracellular domain fused to β3-integrin transmembrane and cytoplasmic domains), human β1-integrin extracellular domain was amplified from Met1 to Ile729 and fused to β3-integrin transmembrane and cytoplasmic domains of β3-integrin-GFP[9]. Then, the GFP was replaced by the sequence of mEOS2. The recombinaisons between the different fragments were integrated in the pLenti-MCS vector (Invitrogen) with the InFusion HD cloning kit (Ozyme). 6His-TM, the trans-membrane domain of the PDGF receptor carrying a 6His tag (pDisplay-AP-6His-CFP-TM)[41] was kindly provided by A. Ting (MIT, Cambridge, MA). For the mEOS2-TM, a PCR of mEOS2 was done on pRSETa-mEOS2 (Addgene) and was used to replace the 6His tag in the 6His-TM at the SfiI / SalI sites. mEos2 Rac1 Cter (CAAX) is the generous gift of A. Gautreau (Laboratoire d'Enzymologie et de Biochimie Structurales, UPR 3082 CNRS, Gif-sur-Yvette, France). The fidelity of all

constructs was verified by sequencing. All other constructs were used as described: GFP-VASP[42] provided by Juergen Wehland (German Research Center for Biotechnology, Braunschweig, Germany).

sptPALM

Cells were imaged at 37°C in an open chamber (Ludin chamber, Life Imaging Services, Switzerland) mounted on an inverted motorized microscope (Nikon Ti, Japan) equipped with a 100x1.45 NA PL-APO objective and a perfect focus system, allowing long acquisition in TIRF illumination mode. For photoactivation localization microscopy, cells expressing mEOS2 tagged constructs were photoactivated using a 405 nm laser (Omicron, Germany) and the resulting photoconverted single molecule fluorescence was excited with a 561 nm laser (Cobolt Jive™, Cobolt, Sweden). Both lasers illuminated the sample simultaneously. Their respective power was adjusted to keep the number of the stochastically activated molecules constant and well separated during the acquisition. To perform sptPALM, laser intensities were tuned in order to keep the single molecule fluorescent during multiple frames before bleaching. The fluorescence was collected by the combination of a dichroic and emission filters (D101-R561 and F39-617 respectively, Chroma, USA) and a sensitive EMCCD (Evolve, Photometric, USA). The acquisition was steered by Metamorph software (Molecular Devices, USA) in streaming mode at 50 frames per second (20 ms exposure time). GFP-paxillin, GFP-VASP were imaged using a conventional GFP filter cube (ET470/40, T495LPXR, ET525/50, Chroma, USA). We used multicolor fluorescent micro-beads (Tetraspeck, Invitrogen) to register long term acquisitions and correct for lateral drifts.

Single molecule segmentation and tracking

A typical single cell sptPALM, acquired with the microscope setup and protocol described above, leads to a set of 20.000 images that further need to be analysed in order to extract molecule localization and dynamics. Single molecule fluorescent spots were localized in each image frame and tracked over time using a combination of wavelet segmentation and simulated annealing algorithms[43,44]. Under the experimental conditions described above, the resolution of the whole system was quantified to 47 nm (Full Width at Half Maximum). This spatial resolution, which depends on the image signal to noise ratio and the segmentation algorithm[45,46], was determined experimentally using fixed samples labelled with mEOS2. To do so, we analysed 130 2D distributions of single molecule positions belonging to long trajectories (more than 50 frames) by bi-dimensional Gaussian fitting, the resolution being determined as $2.3\sigma_{xy}$, where σ_{xy} is the pointing accuracy. For the trajectory analysis, FAs were identified by wavelet image segmentation of the GFP-paxillin or GFP-VASP signal. The corresponding binary mask was then used to sort single particle data analyses to specific regions.

We analyzed trajectories lasting at least 20 points (400 ms≤, 8% of the trajectories) with a custom routine written for Matlab using the mean squared displacement MSD computed as (Eq. 1):

$$MSD(t = n \cdot \Delta t) = \frac{\sum_{i=1}^{N-n}(x_{i+n} - x_i)^2 + (y_{i+n} - y_i)^2}{N - n} \qquad Eq.1$$

where x_i and y_i are the coordinates of the label position at time $i \cdot \Delta t$. We defined the measured diffusion coefficient D as the slope of the affine regression line fitted to the $n = 1$ to 4 values of the $MSD(n \cdot \Delta t)$. The MSD was computed then fitted on a duration equal to 60% (minimum of 12 points, 240 ms) of the whole stretch by (Eq 2):

$$MSD(t) = \frac{4r_{conf}^2}{3}\left(1 - e^{-t/\tau}\right) \qquad Eq.2$$

where r_{conf} is the measured confinement radius and τ the time constant ($\tau = r_{conf}^2/3D_{conf}$). Trajectories were sorted in 3 groups, immobile, confined diffusion and free-diffusion. Immobile trajectories were defined as trajectories with D<0.008 $\mu m^2.s^{-1}$, corresponding to molecules which explored an area inferior to the one defined by the image spatial resolution ~$(0.05\mu m)^2$ during the time used to fit the initial slope of the MSD[47] (4 points, 80 ms): D=$(0.05\mu m)^2$/(4x4x0.02s)~0.008 $\mu m^2.s^{-1}$. To separate trajectories displaying free-diffusion from confined diffusion, we used the time constant τ calculated for each trajectory. We sorted trajectories displaying free-diffusion from confined diffusion using the time constant τ defined above. Confined trajectories were defined as trajectories with a time constant τ inferior to half the time interval used to compute the MSD (120 ms). On the contrary, free-diffusing trajectories were defined as trajectories with a time constant superior to half the time interval used to compute the MSD (120 ms). The result of this sorting procedure is illustrated in Fig. 1b,d which shows the variation of the MSD over the time interval for each population: flat for immobile trajectories (red), reaching a plateau for confined trajectories (green), and linear for diffusive trajectories (purple)(see Fig. 1b,d).

Localization of immobilization zones and measurement of their durations

Immobilization zones correspond to locations where bursts of mEOS2 fluorescence were repeatedly detected during the course of a sptPALM sequence (Supplementary Fig. S3). The duration of immobilization zones was defined as the time interval between the first and the last mEOS2 detection at the same location (Supplementary Fig. S3). More precisely, we first generated a sptPALM intensity image for each cell (20000 frames, 400s). Then, the images were processed with a wavelet-based segmentation algorithm to define immobilization zones and generate the corresponding binary mask. Then from the same set of data, we generated a super-resolved time-lapse movie (frame rate 1s) and we used the binary mask, to study time evolution of the fluorescence emission within immobilization zones. To eliminate the events stemming from molecules crossing the immobilization area, single molecule detections were taken into account only if at least 3 fluorescent events were occurring within 1 s. To account for blinking[48] of mEOS2, up to 20 s off-times were allowed in a time trace for defining an immobilization event. As a control, the same procedure was applied to β3-WT in fixed cells where apparent finite time traces are imposed by mEOS2 photo-physics (bleaching and blinking). The duration measured in this case are systematically longer than in live cells, and well above lifetimes measured for conditions shortening integrin immobilization.

Probes functionalization and TrisNTA-ATTO647N synthesis

We performed SMT using a small ATTO647N probes functionalized with Ni^{2+} tris-nitrilotriacetic acid (TrisNTA), a high affinity ligand for 6-histidine (6His) tag[24,25] fused to the extracellular N-terminal of β3-integrin WT, mutants, and TM. Because the dye/linker combinations were small (2 nm) and monovalent, β3-integrins were efficiently labeled (Supplementary Fig. S4) and tracked (Supplementary Fig. S5) in crowded and confined FAs at the cell-substrate interface. TrisNTA, synthesized as previously described[24,49], was coupled on solid phase to the N terminus of the proline linker peptide, PPPPCA. After deprotection and cleavage from the resin, the cysteine residue was labeled with ATTO647N-maleimide (ATTO-TEC GmbH, Siegen, Germany) via standard thiol chemistry. Products were purified via reversed-phase C_{18} HPLC. The trisNTA-ATTO647N was loaded with nickel and its concentration was determined via the absorption of the fluorophore as described[24].

SMT

A standard single molecule epifluorescence microscope was used for detecting individual fluorophores[47]. In brief, the 633 nm line of a HeNe laser in the TIRF mode was used to excite individual ATTO647N molecules, an organic dye, which bears remarkable photostability properties[25,31]. Samples were mounted on an inverted microscope (IX71 Olympus) equipped with a high 100x objective (NA = 1.45) and a CCD camera (Cascade 128, Roper Scientific). We used an acquisition frequency of 5Hz to further increase the number of long trajectories (>10 s). In each image of the recorded sequence, the single fluorescent probes appear as diffraction-limited bright spots. Images were analyzed using the segmentation and tracking program described above for sptPALM in order to retrieve single ATTO647N localizations and trajectories. The resolution of the whole system was quantified to 48 nm (Full Width at Half Maximum). For the trajectory analysis, FAs were identified by wavelet image segmentation of the GFP-VASP signal. Trajectories were segmented according to their location inside or outside FAs. Trajectories were analyzed using a custom Matlab routine[50]. We analyzed the degree of molecule mobility by measuring the molecule displacement steps. Probability distributions of the squared displacement steps were used as a statistical approach to characterize the mobility behaviors of β3-integrin sub-populations (see ref. [47]). Within the spatial resolution of our experimental conditions, displacements steps lower than $(0.048\ \mu m)^2=2.3\ 10^{-3}\ \mu m^2$ are assigned to immobile molecules. Both inside and outside FAs, we found two populations: one including immobile and slowly mobile molecules, and the other displaying faster mobility (Supplementary Fig. S5). The fractions of these two populations, for all conditions, were in agreement with the fraction of immobilization measured by sptPALM (Supplementary Fig. S5e-g).

STED

MEFs expressing human β3-integrin-GFP were spread on FN coated glass coverslips. MEFs were fixed for 15 min in 4% paraformaldehyde and permeabilized with 0.2 % triton X-100 for 10 min. Then we performed immunostaining of: (i) endogenous mouse β1-integrin with monoclonal antibody (clone 9EG7 from BD Pharmingen, NJ, USA) detected by ATTO647N labeled secondary antibody (rat); or (ii) transfected human β3-integrin with a monoclonal anti human integrin αvBeta3 (clone LM609, from Millipore) detected by ATTO647N labeled secondary antibody (mouse). We used a commercial STED microscope Leica DMI6000 inverted TCS SP5 AOBS (Leica, Germany) to obtain super-resolved images of β1-integrin or β3-integrin. Using the regular confocal mode, we acquired β3-integrin-GFP images to localize FAs.

Statistical analysis.

Averages and SEM were calculated and are shown in the graphs. Respective n values are shown in the figure legends and in Supplementary table S1-3. The indicated P values were obtained with two-tailed Student's t -tests. Resulting P values are indicated as follows n.s when $P > 0.05$; * when $0.01<P<0.05$; ** when $0.001<P<0.01$; *** when $P<0.0001$.

References

1 Geiger, B., Spatz, J.P., & Bershadsky, A.D., Environmental sensing through focal adhesions. *Nat Rev Mol Cell Biol* 10 (1), 21-33 (2009).

2 Shattil, S.J., Kim, C., & Ginsberg, M.H., The final steps of integrin activation: the end game. *Nat Rev Mol Cell Biol* 11 (4), 288-300 (2010).

3 Danen, E.H., Sonneveld, P., Brakebusch, C., Fassler, R., & Sonnenberg, A., The fibronectin-binding integrins alpha5beta1 and alphavbeta3 differentially modulate RhoA-GTP loading, organization of cell matrix adhesions, and fibronectin fibrillogenesis. *J Cell Biol* 159 (6), 1071-1086 (2002).

4 Zamir, E. *et al.*, Dynamics and segregation of cell-matrix adhesions in cultured fibroblasts. *Nat Cell Biol* 2 (4), 191-196 (2000).

5 Roca-Cusachs, P., Gauthier, N.C., Del Rio, A., & Sheetz, M.P., Clustering of alpha(5)beta(1) integrins determines adhesion strength whereas alpha(v)beta(3) and talin enable mechanotransduction. *Proc Natl Acad Sci U S A* 106 (38), 16245-16250 (2009).

6 Kanchanawong, P. *et al.*, Nanoscale architecture of integrin-based cell adhesions. *Nature* 468 (7323), 580-584 (2010).

7 Choquet, D., Felsenfeld, D.P., & Sheetz, M.P., Extracellular matrix rigidity causes strengthening of integrin-cytoskeleton linkages. *Cell* 88 (1), 39-48 (1997).

8 Jiang, G., Giannone, G., Critchley, D.R., Fukumoto, E., & Sheetz, M.P., Two-piconewton slip bond between fibronectin and the cytoskeleton depends on talin. *Nature* 424 (6946), 334-337 (2003).

9 Cluzel, C. *et al.*, The mechanisms and dynamics of (alpha)v(beta)3 integrin clustering in living cells. *J Cell Biol* 171 (2), 383-392 (2005).

10 Brown, C.M. *et al.*, Probing the integrin-actin linkage using high-resolution protein velocity mapping. *J Cell Sci* 119 (Pt 24), 5204-5214 (2006).

11 Hu, K., Ji, L., Applegate, K.T., Danuser, G., & Waterman-Storer, C.M., Differential transmission of actin motion within focal adhesions. *Science* 315 (5808), 111-115 (2007).

12 Betzig, E. *et al.*, Imaging intracellular fluorescent proteins at nanometer resolution. *Science* 313 (5793), 1642-1645 (2006).

13 Manley, S. *et al.*, High-density mapping of single-molecule trajectories with photoactivated localization microscopy. *Nat Methods* 5, 155 (2008).

14 Luo, B.H., Springer, T.A., & Takagi, J., Stabilizing the open conformation of the integrin headpiece with a glycan wedge increases affinity for ligand. *Proc Natl Acad Sci U S A* 100 (5), 2403-2408 (2003).

15 O'Toole, T.E., Ylanne, J., & Culley, B.M., Regulation of integrin affinity states through an NPXY motif in the beta subunit cytoplasmic domain. *J Biol Chem* 270 (15), 8553-8558 (1995).

16 Tadokoro, S. *et al.*, Talin binding to integrin beta tails: a final common step in integrin activation. *Science* 302 (5642), 103-106 (2003).

17 Loftus, J.C. *et al.*, A beta 3 integrin mutation abolishes ligand binding and alters divalent cation-dependent conformation. *Science* 249 (4971), 915-918 (1990).

18 McCleverty, C.J., Lin, D.C., & Liddington, R.C., Structure of the PTB domain of tensin1 and a model for its recruitment to fibrillar adhesions. *Protein Sci* 16 (6), 1223-1229 (2007).

19 Kiema, T. *et al.*, The molecular basis of filamin binding to integrins and competition with talin. *Mol Cell* 21 (3), 337-347 (2006).

20 Legate, K.R. & Fassler, R., Mechanisms that regulate adaptor binding to beta-integrin cytoplasmic tails. *J Cell Sci* 122 (Pt 2), 187-198 (2009).

21 Giannone, G., Jiang, G., Sutton, D.H., Critchley, D.R., & Sheetz, M.P., Talin1 is critical for force-dependent reinforcement of initial integrin-cytoskeleton bonds but not tyrosine kinase activation. *J Cell Biol* 163 (2), 409-419 (2003).
22 Zhang, X. *et al.*, Talin depletion reveals independence of initial cell spreading from integrin activation and traction. *Nat Cell Biol* 10 (9), 1062-1068 (2008).
23 Shroff, H., Galbraith, C.G., Galbraith, J.A., & Betzig, E., Live-cell photoactivated localization microscopy of nanoscale adhesion dynamics. *Nat Methods* 5 (5), 417-423 (2008).
24 van der Does, C., Presenti, C., Schulze, K., Dinkelaker, S., & Tampe, R., Kinetics of the ATP hydrolysis cycle of the nucleotide-binding domain of Mdl1 studied by a novel site-specific labeling technique. *J Biol Chem* 281 (9), 5694-5701 (2006).
25 Giannone, G. *et al.*, Dynamic superresolution imaging of endogenous proteins on living cells at ultra-high density. *Biophys J* 99 (4), 1303-1310 (2010).
26 Pankov, R. *et al.*, Integrin dynamics and matrix assembly: tensin-dependent translocation of alpha(5)beta(1) integrins promotes early fibronectin fibrillogenesis. *J Cell Biol* 148 (5), 1075-1090 (2000).
27 Giannone, G., Mege, R.M., & Thoumine, O., Multi-level molecular clutches in motile cell processes. *Trends Cell Biol* 19 (9), 475-486 (2009).
28 Friedland, J.C., Lee, M.H., & Boettiger, D., Mechanically activated integrin switch controls alpha5beta1 function. *Science* 323 (5914), 642-644 (2009).
29 Huveneers, S., Truong, H., Fassler, R., Sonnenberg, A., & Danen, E.H., Binding of soluble fibronectin to integrin alpha5 beta1 - link to focal adhesion redistribution and contractile shape. *J Cell Sci* 121 (Pt 15), 2452-2462 (2008).
30 Anthis, N.J., Wegener, K.L., Critchley, D.R., & Campbell, I.D., Structural diversity in integrin/talin interactions. *Structure* 18 (12), 1654-1666 (2010).
31 Westphal, V. *et al.*, Video-rate far-field optical nanoscopy dissects synaptic vesicle movement. *Science* 320 (5873), 246-249 (2008).
32 Worth, D.C. *et al.*, Alpha v beta3 integrin spatially regulates VASP and RIAM to control adhesion dynamics and migration. *J Cell Biol* 189 (2), 369-383 (2010).
33 Arias-Salgado, E.G. *et al.*, Src kinase activation by direct interaction with the integrin beta cytoplasmic domain. *Proc Natl Acad Sci U S A* 100 (23), 13298-13302 (2003).
34 Millon-Fremillon, A. *et al.*, Cell adaptive response to extracellular matrix density is controlled by ICAP-1-dependent beta1-integrin affinity. *J Cell Biol* 180 (2), 427-441 (2008).
35 del Rio, A. *et al.*, Stretching single talin rod molecules activates vinculin binding. *Science* 323 (5914), 638-641 (2009).
36 Vogel, V., Mechanotransduction involving multimodular proteins: converting force into biochemical signals. *Annu Rev Biophys Biomol Struct* 35, 459-488 (2006).
37 Kong, F., Garcia, A.J., Mould, A.P., Humphries, M.J., & Zhu, C., Demonstration of catch bonds between an integrin and its ligand. *J Cell Biol* 185 (7), 1275-1284 (2009).
38 Smith, M.L. *et al.*, Force-induced unfolding of fibronectin in the extracellular matrix of living cells. *PLoS Biol* 5 (10), e268 (2007).
39 Parsons, M., Messent, A.J., Humphries, J.D., Deakin, N.O., & Humphries, M.J., Quantification of integrin receptor agonism by fluorescence lifetime imaging. *J Cell Sci* 121 (3), 265-271 (2008).
40 Plançon, S., Morel-Kopp, M.C., Schaffner-Reckinger, E., Chen, P., & Kieffer, N., Green fluorescent protein (GFP) tagged to the cytoplasmic tail of alphaIIb or beta3 allows the expression of a fully functional integrin alphaIIb(beta3): effect of beta3GFP on alphaIIb(beta3) ligand binding. *Biochem. J.* 357 (2), 529-536 (2001).

41 Chen, I., Howarth, M., Lin, W., & Ting, A.Y., Site-specific labeling of cell surface proteins with biophysical probes using biotin ligase. *Nat Meth* 2 (2), 99-104 (2005).
42 Rottner, K., Behrendt, B., Small, J.V., & Wehland, J., VASP dynamics during lamellipodia protrusion. *Nat Cell Biol* 1 (5), 321-322 (1999).
43 Racine, V. *et al.*, Multiple-target tracking of 3D fluorescent objects based on simulated annealing. *IEEE International Symposium on Biomedical Imaging*, 1020-1023 (2006).
44 Racine, V. *et al.*, Visualization and quantification of vesicle trafficking on a three-dimensional cytoskeleton network in living cells. *J Microsc* 225 (Pt 3), 214-228 (2007).
45 Kubitscheck, U., Kuckmann, O., Kues, T., & Peters, R., Imaging and tracking of single GFP molecules in solution. *Biophys J* 78 (4), 2170-2179 (2000).
46 Cheezum, M.K., Walker, W.F., & Guilford, W.H., Quantitative comparison of algorithms for tracking single fluorescent particles. *Biophys J* 81 (4), 2378-2388 (2001).
47 Tardin, C., Cognet, L., Bats, C., Lounis, B., & Choquet, D., Direct imaging of lateral movements of AMPA receptors inside synapses. *Embo J* 22 (18), 4656-4665 (2003).
48 Annibale, P., Scarselli, M., Kodiyan, A., & Radenovic, A., Photoactivatable Fluorescent Protein mEos2 Displays Repeated Photoactivation after a Long-Lived Dark State in the Red Photoconverted Form. *The Journal of Physical Chemistry Letters* 1 (9), 1506-1510 (2010).
49 Lata, S., Gavutis, M., Tampe, R., & Piehler, J., Specific and stable fluorescence labeling of histidine-tagged proteins for dissecting multi-protein complex formation. *J Am Chem Soc* 128 (7), 2365-2372 (2006).
50 Groc, L. *et al.*, Surface trafficking of neurotransmitter receptor: comparison between single-molecule/quantum dot strategies. *J Neurosci* 27 (46), 12433-12437 (2007).

Acknowledgements

We thank C. Breillat, A. Frouin, D. Bouchet, and P. Gonzales for technical assistance; M.P. Sheetz, O. Thoumine, J. Petersen, B. Fourcade, M. Block, L. Duchesne, D.G. Fernig for helpful discussions; M. Humphries, N. Kieffer, J. Wehland and A. Gautreau for the gift of reagents; P. Legros and C. Poujol (Bordeaux Imaging Center) for STED imaging. We acknowledge financial support from the French Ministry of Research and CNRS, ANR grant Nanomotility (GG, BL, OR), Association pour la Recherche sur le Cancer ARC (OR), Conseil Régional Aquitaine, Fondation pour la Recherche Médicale, the ERC Program n° 232942 Nano-Dyn-Syn (DC,BL) and n° 235552 Glutraf (DN), The Cancer and Polio Research Fund (LD, DGF), Human Frontiers Science Programme (LD, DGF, BL), the North West Cancer Research Fund (DGF), The Ligue National contre le Cancer - équipe labellisée 2010 (CAR, OD).

Author Contributions

OR and GG conceptualized and performed the sptPALM and STED experiments. VO, CL, LC and BL conceptualized and developed the SMT set-up. GG performed SMT experiments. VG and RT designed and synthesized the TrisNTA-ATTO647N. DN and JBS developed the sptPALM set-up. JBS developed the analytical tools for sptPALM. VO, CL and LC developed the analytical tools for SMT. OD and CAR contributed valuable scientific advices and developed the β1-integrin-mEOS2 and chimeric integrin constructs. LC, DC, BL and GG coordinated the study. OR and GG wrote the manuscript and supplement. All authors discussed the results and commented on the manuscript.

Author Information Correspondence and requests for materials should be addressed to G.G (Gregory.giannone@u-bordeaux2.fr).

Figure legends

Figure 1. β3-integrins preferential immobilization and slower free-diffusion within FAs are triggered by integrin specific interactions

(a) sptPALM of β3-WT-mEOS2 in MEFs. Trajectories overlaid on FAs (gray) are color-coded to show their diffusion modes: diffusive (purple), confined (green) and immobile (red). Boxed area (left), region shown on the right, scale bars, 1 μm. **(b)** Variation of the MSD over time for trajectories inside (plain) and outside FAs (dashed) with the same color-code as in **a** (mean ± SEM for trajectories). **(c,d)** Same as **a** and **b** for CAAX. **(e)** Fraction of diffusive, confined and immobile populations for β3-WT (black), TM (yellow) and CAAX (magenta) inside and outside FAs (mean ± SEM for cells). **(f,g)** Distribution of LOG(D) inside and outside FAs (mean for cells). The gray areas including D values inferior to 0.008 $\mu m^2.s^{-1}$ correspond to immobile trajectories. **(h)** Radii of confinements (mean ± SEM for trajectories). **(i)** D for confined events (mean ± SEM for trajectories). **(j)** D for free-diffusive events (mean ± SEM for trajectories). β3-WT (9 cells, n=23804 trajectories), TM (5 cells, n=14256 trajectories) and CAAX (6 cells, n=8008 trajectories) (also see Supplementary table S1).). When indicated, statistical significances were obtained with a two-tailed Student's t-test comparing inside FAs, the different conditions vs. the β3-WT condition and outside FAs, comparing inside vs. outside values for each given condition. Resulting P values are indicated as follows n.s when $P > 0.05$; * when $0.01<P<0.05$; ** when $0.001<P<0.01$; *** when $P<0.0001$.

Figure 2. Conditions promoting integrin activation correlate with integrin immobilization which requires simultaneous FN and ABP binding, while initiation depends preferentially on ABP

(a) sptPALM of β3-N305T. Trajectories overlaid on FAs (gray) are color-coded to show their diffusion modes: diffusive (purple), confined (green) and immobile (red). Boxed area (left), region shown on the right, scale bars, 1 μm. **(b,c)** Distribution of LOG(D) inside and outside FAs for β3-WT (black), β3-N305T (blue) and Mn^{2+} stimulated β3-WT (light blue) (mean for cells). The gray areas including D values inferior to 0.008 $\mu m^2.s^{-1}$ correspond to immobile trajectories. **(d)** Fraction of diffusive, confined and immobile populations (mean ± SEM for cells) and **(e)** D for free-diffusive events (mean ± SEM for trajectories). **(f)** sptPALM of β3-Y747A. Trajectories overlaid on FAs (gray) are color-coded to show their diffusion modes:

diffusive (purple), confined (green) and immobile (red). Boxed area (left), region shown on the right, scale bars, 1 μm. **(g,h)** Distribution of LOG(D) inside and outside FAs for β3-WT (black), β3-D119Y (green) and β3-Y747A (red) inside and outside FAs (mean for cells). The gray areas including D values inferior to 0.008 $\mu m^2.s^{-1}$ correspond to immobile trajectories. **(i)** Fraction of diffusive, confined and immobile populations (mean ± SEM for trajectories) and **(j)** D for free-diffusive events (mean ± SEM for trajectories). β3-N305T (7 cells, 8876 trajectories), β3-WT + Mn^{2+} (4 cells, 12910 trajectories), β3-D119Y (6 cells, 23784 trajectories), β3-Y747A (6 cells, 17894 trajectories) (also see Supplementary table S1). When indicated, statistical significances were obtained with a two-tailed Student's t-test comparing inside FAs, the different conditions vs. the β3-WT condition and outside FAs, comparing inside vs. outside values for each given condition. Otherwise, a black line indicates which pair of conditions was compared.

Figure 3. Integrins undergo repeated cycles of slow free-diffusion and immobilization within FAs

(a) High resolution image of β3-WT density in a FA (inset: labeled with GFP-paxillin) obtained from a sptPALM sequence (duration: 400s). Boxed area (left) is shown at right highlighting β3-WT immobilization zones (arrow). Kymograph (right) generated from sptPALM super-resolution time-lapse[23] along the length of the FA (inset, dashed lines encompassing the FA). The duration of immobilization zones was defined as the time interval between the first and the last mEOS2 detection (dashed lines) at the same location. In between signal intermittencies could be attributed to on-off blinking characteristic of single mEOS2 (see Methods). **(b)** Same as **a** but for β3-Y747A. **(c)** Cumulative distribution of immobilization duration measured from sptPALM, inside (left) and outside (right) FAs for: β3-WT (black, plain, 9 cells, 10821 immobilization events), β3-WT in fixed cells (black, dashed, 7 cells, 5610 immobilization events), β3-N305T (blue, 7 cells, 5396 immobilization events), β3-D119Y (green, 6 cells, 5588 immobilization events), β3-Y747A (red, 5 cells, 2895 immobilization events) and CAAX (magenta, 6 cells, 1239 immobilization events). **(d)** SMT of 6His-β3-WT using TrisNTA-ATTO647N. Trajectory (14 s) overlaid on FAs is color-coded from slow (red) to fast (blue) displacement steps and displays transitions between fast free-diffusion (1), slow free-diffusion (2) and confinement (3). Boxed area (left), region shown on the middle. Right: instantaneous displacement ($STEP^2$) versus time along the described trajectory. **(e)** Same as **d** for a trajectory (17 s) overlaid on FAs displaying transitions between

confinement (1), slow free-diffusion (2) and confinement (3). (also see Supplementary Fig. S4,S5).

Figure 4. Differential nano-scale organization of β3- and β1-integrins in FAs is determined by the extracellular binding to FN

(a) sptPALM of β1-WT. Trajectories overlaid on FAs (gray) are color-coded to show their diffusion modes: diffusive (purple), confined (green) and immobile (red). Boxed area (left), region shown on the right, scale bars, 1 μm. **(b,c)** Distribution of LOG(D) inside and outside FAs for β3-WT (black), β1-WT (brown), β1-D130Y (green) and β1-Y783A (red) (mean for cells). The gray areas including D values inferior to 0.008 $\mu m^2.s^{-1}$ correspond to immobile trajectories. **(d)** Fraction of diffusive, confined and immobile populations (mean ± SEM for cells) and **(e)** D for free-diffusive events (mean ± SEM for trajectories) for β3-WT (black), β1-WT (brown), β1-D130Y (green) and β1-Y783A (red) but also for the chimeras β3ext-β1int (black) and β1ext-β3int (brown). **(f)** Ratio of inside versus outside FAs detections for β3-integrins (black), β1-integrins (brown), but also for chimeric β3ext-β1int (black) and β1ext-β3int (brown). **(g)** High resolution sptPALM image of β3-WT density in FAs. Boxed area (left) is shown at right. **(h)** Same as **g** for β1-WT. β1-WT (9 cells, 21749 trajectories), β1-D130Y (10 cells, 13593 trajectories), β1-Y783A (7 cells, 7665 trajectories), β3ext-β1int (8 cells, 10756 trajectories), β1ext-β3int (6 cells, 8848 trajectories) (also see Supplementary table S1). When indicated, statistical significances were obtained with a two-tailed Student's t-test comparing inside FAs, the different conditions vs. the β1-WT condition and outside FAs, comparing inside vs. outside values for each given condition. Otherwise, a black line indicates which pair of conditions was compared.

Figure 5. The differential transmission of actin motion for β3- and β1-integrins within FAs are determined by the extracellular binding to FN.

(a) High resolution image of β3-WT density in FAs (right) labeled by GFP-paxillin (left). Scale bar, 2 μm. **(b)** Kymograph obtained from super-resolution time-lapses (frame rate 4s) along a FA highlighted with white dashed lines in **a** where the horizontal axis represents spatial dimension and the vertical axis represents time. Kymographs allow the measurement of long term motions of immobilized integrins within FAs. β3-WT long term motions are highlighted by dashed white lines with the corresponding velocity in nm/s. **(c)** Same as **a** for β1-WT. **(d)** Same as **b** for β1-WT. **(e)** Distribution of rearward speed for β3-WT (black) and

β1-WT (brown). **(f)** Same as **e** for chimeric β3ext-β1int (black) and β1ext-β3int (brown). β1-WT (8 cells, 489 events), β3-WT (5 cells, 346 events); β1ext-β3int (8 cells, 603 events), β3ext-β1int (9 cells, 842 events).

Figure 1-Giannone

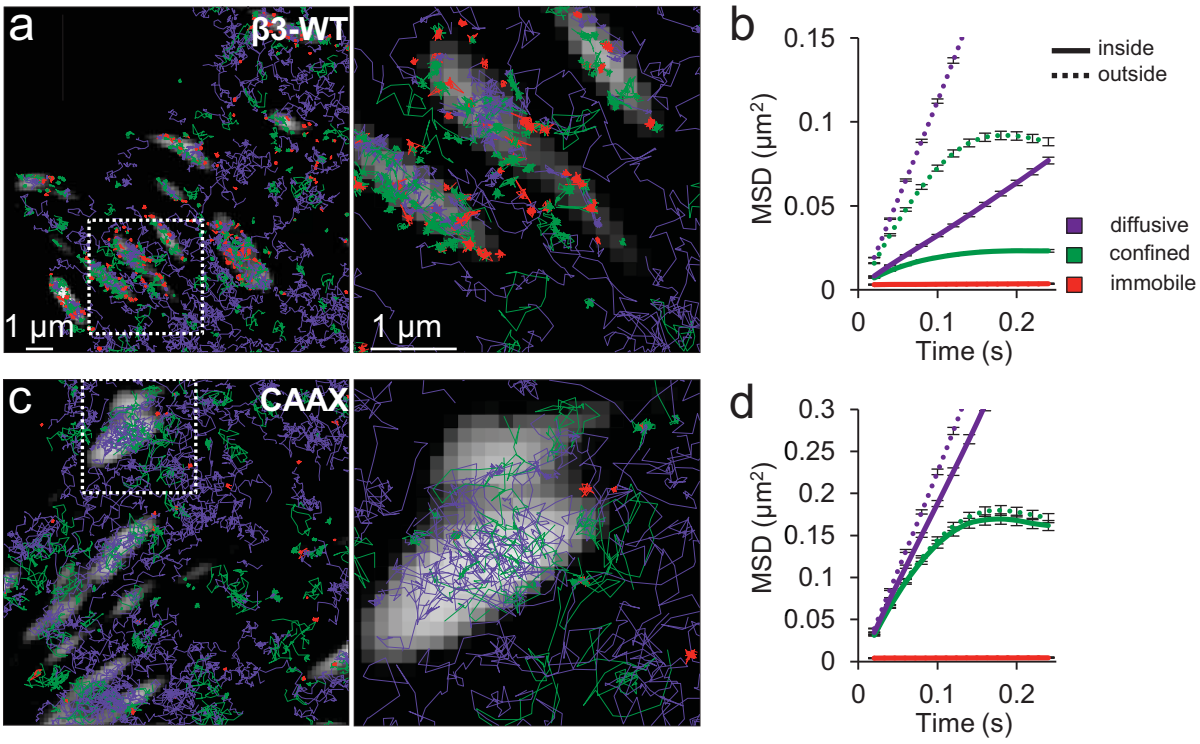

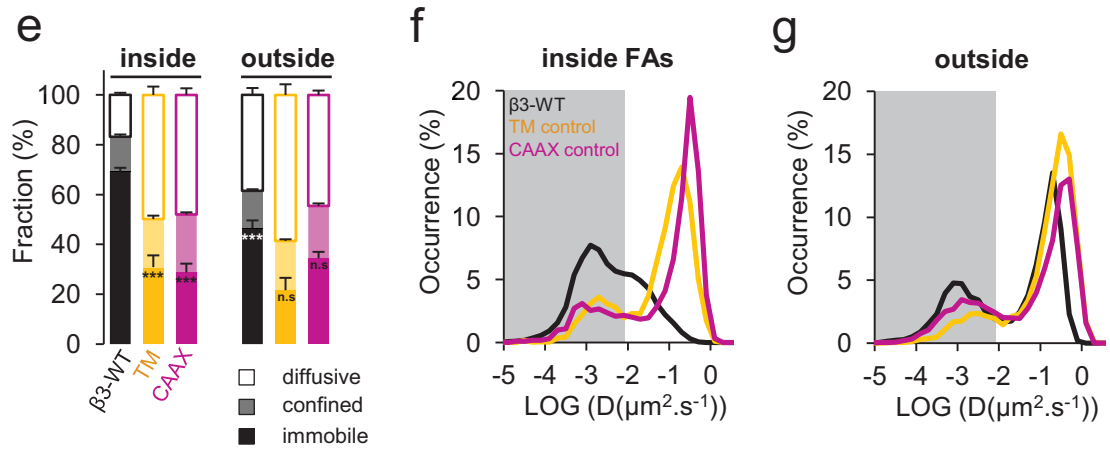

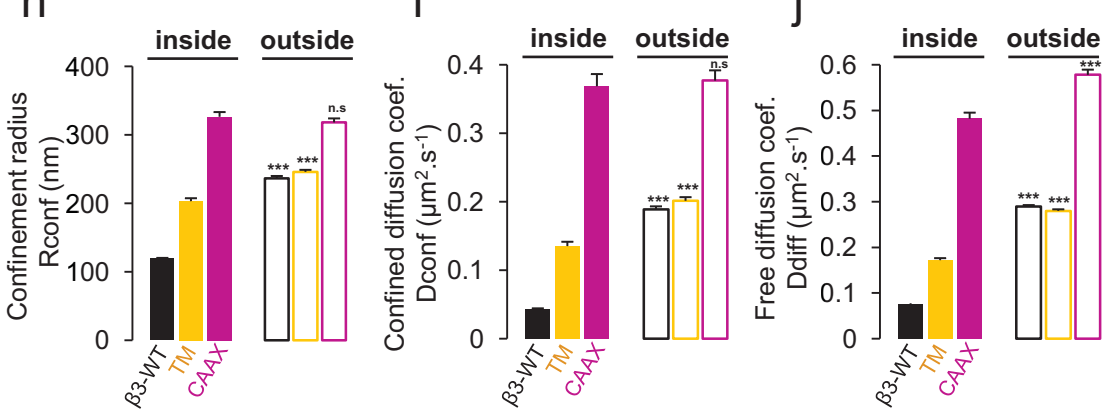

Figure 2-Giannone

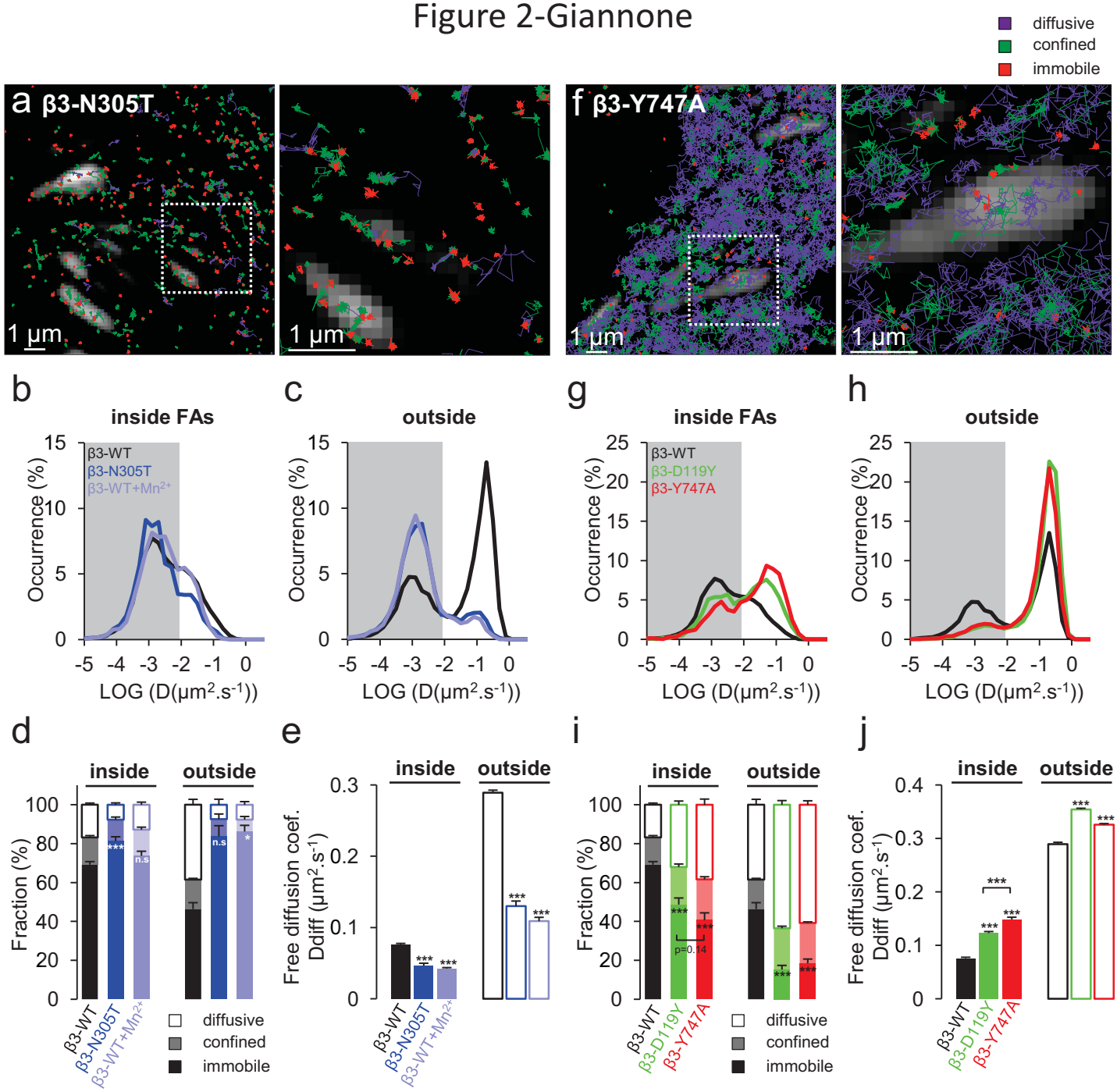

Figure 3-Giannone

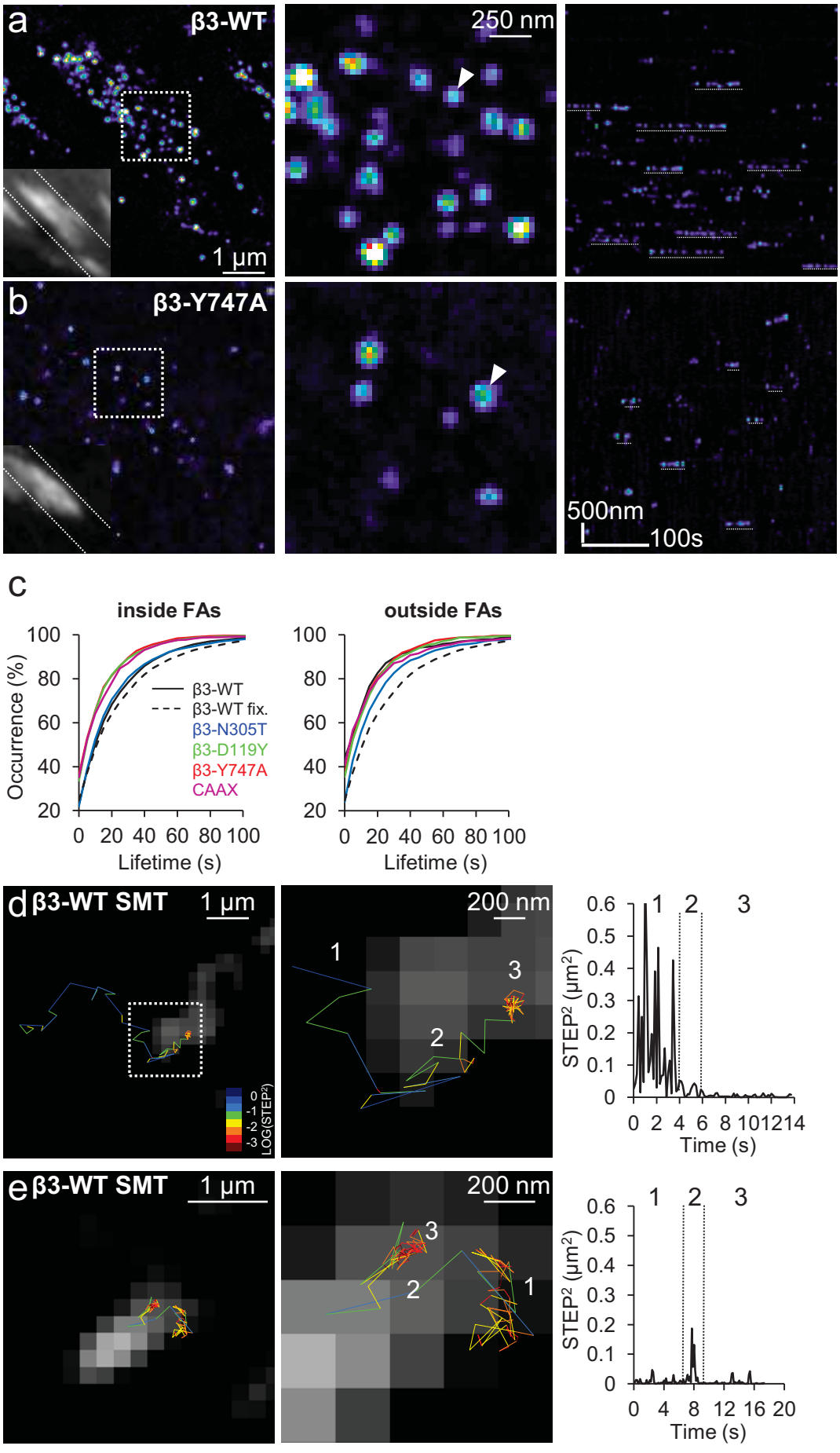

Figure 4-Giannone

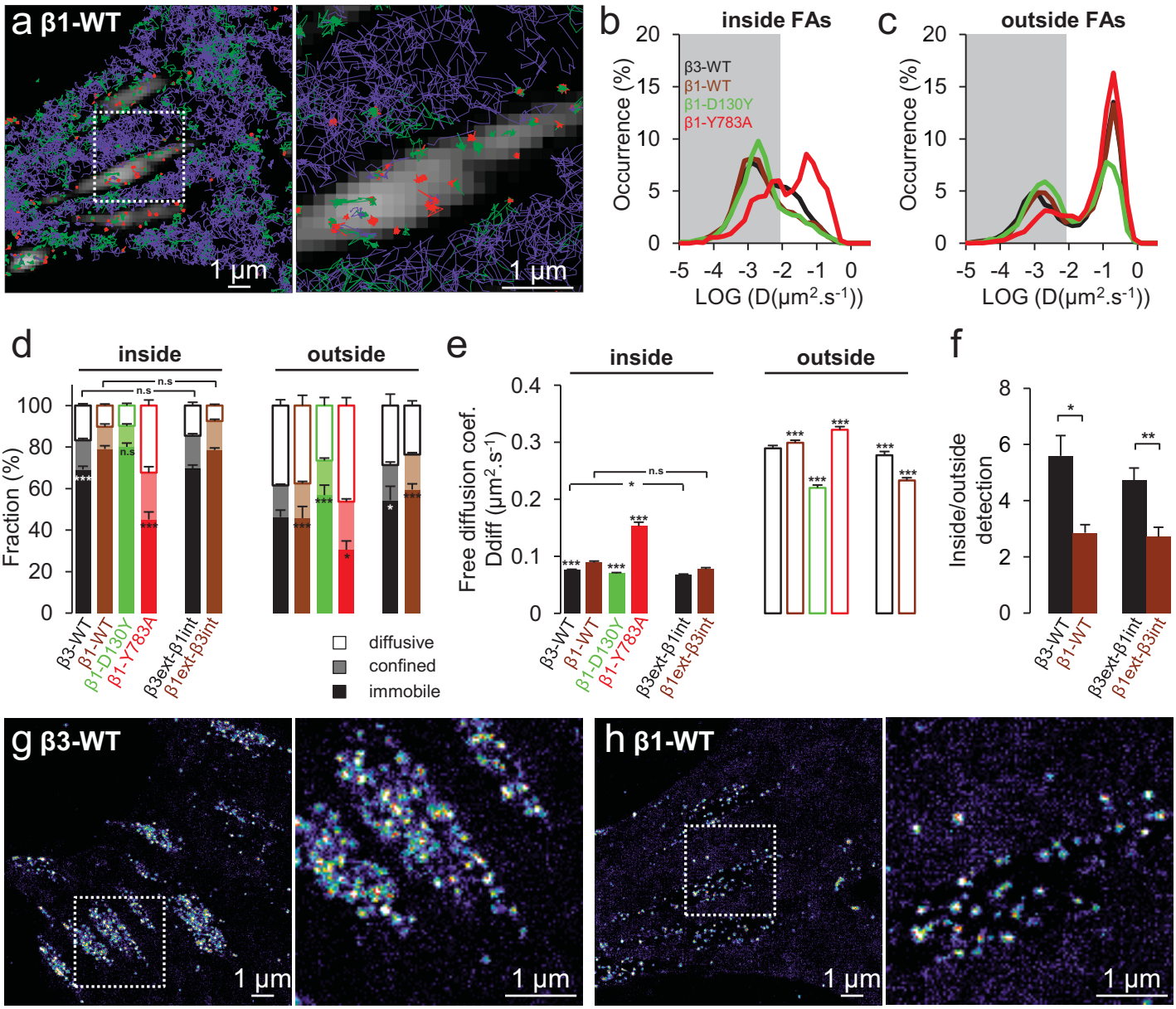

Figure 5-Giannone

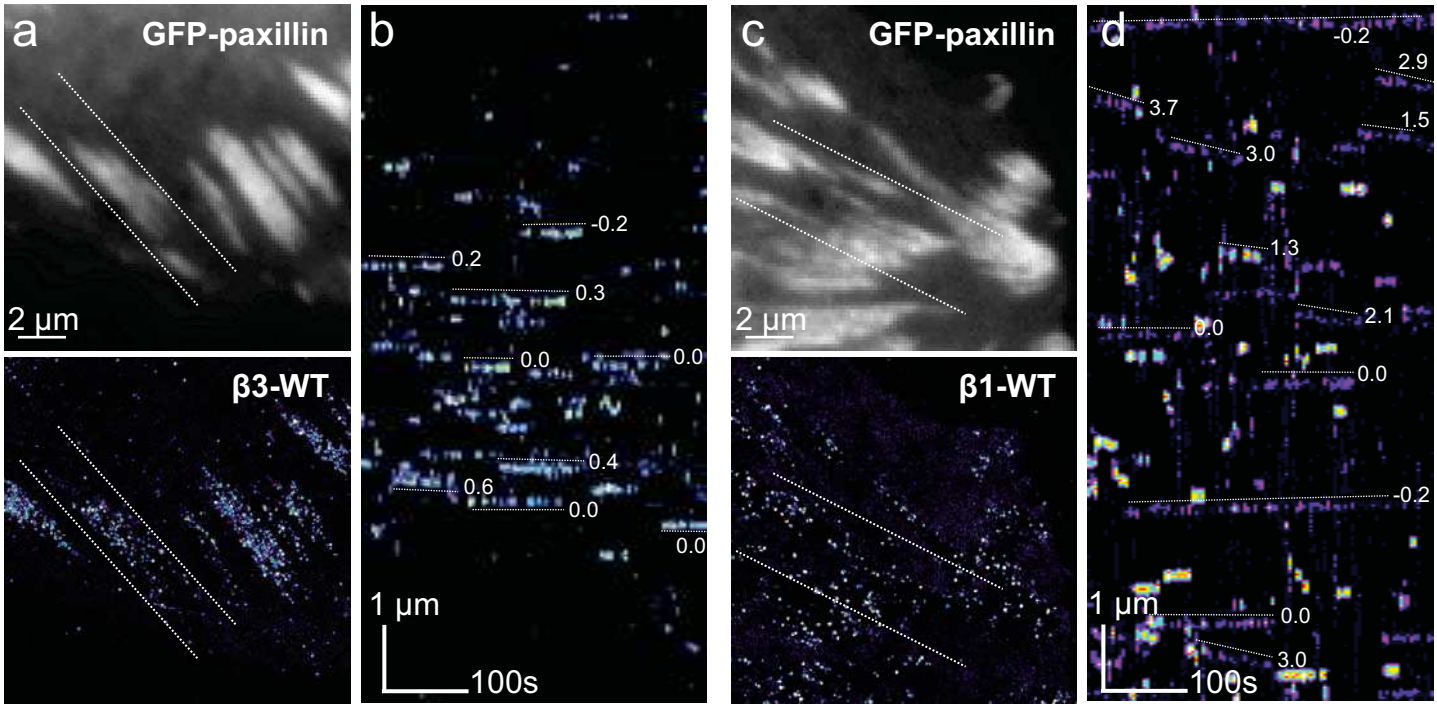

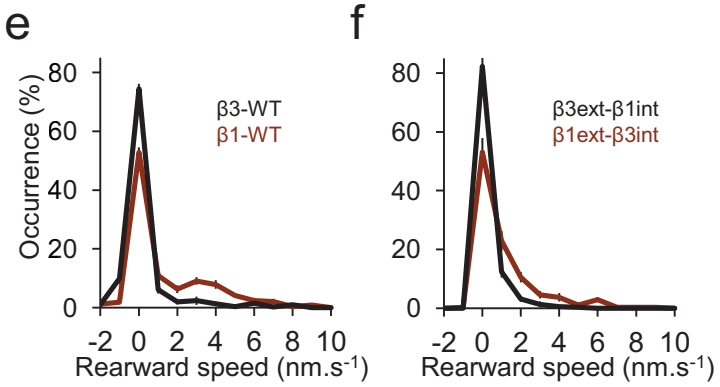

Supplementary Information

Supplementary figure legends

Figure S1. Motion parameters of confined diffusion for β3-WT, Mn2+ stimulated β3-WT, β3-N305T, β3-D119Y and β3-Y747A

Motion parameters extracted from sptPALM experiments. **(a)** D for confined events (mean ± SEM for trajectories) for β3-WT (black), β3-N305T (blue) and Mn^{2+} stimulated β3-WT (light blue) inside and outside FAs. **(b)** Radii of confinements (mean ± SEM for trajectories). **(c)** D for confined events (mean ± SEM for trajectories) for β3-WT (black), β3-D119Y (green) and β3-Y747A (red) inside and outside FAs. **(d)** Radii of confinements (mean ± SEM for trajectories). β3-WT (9 cells, n=23804 trajectories), β3-N305T (7 cells, 8876 trajectories), β3-WT + Mn^{2+} (4 cells, 12910 trajectories), β3-D119Y (6 cells, 23784 trajectories), β3-Y747A (6 cells, 17894 trajectories) (also see Supplementary table S1). When indicated, statistical significances were obtained with a two-tailed Student's t-test comparing inside FAs, the different conditions vs. the β3-WT condition and outside FAs, comparing inside vs. outside values for each given condition. Otherwise, a black line indicates which pair of conditions was compared.

Figure S2. Conditions promoting integrin activation correlate with integrin immobilization which requires simultaneous FN and ABP binding, while initiation depends preferentially on ABP binding

Motion parameters extracted from sptPALM for β3-integrins in experiments where FAs were reported using GFP-VASP instead of GFP-paxillin. **(a)** Fraction of diffusive, confined and immobile populations for β3-WT (black), β3-D119Y (green) and β3-Y747A (red), β3-N305T (blue) inside and outside FAs (mean ± SEM for cells). **(b)** Radii of confinements (mean ± SEM for trajectories). **(c)** D for confined events (mean ± SEM for trajectories). **(d)** D for free-diffusive events (mean ± SEM for trajectories). β3-WT (10 cells, n=15798 trajectories), β3-N305T (4 cells, n=3510 trajectories), β3-D119Y (8 cells, n=20130 trajectories), β3-Y747A (5 cells, n=17089 trajectories) (also see Supplementary table S2).

Motion parameters extracted from sptPALM for β3-integrins in β3-integrin$^{-/-}$ MEFs. FAs were reported using GFP-paxillin. **(e)** Fraction of diffusive, confined and immobile

populations for β3-WT (black), β3-D119Y (green) and β3-Y747A (red), β3-N305T (blue) inside and outside FAs (mean ± SEM for cells). **(f)** Radii of confinements (mean ± SEM for trajectories). **(g)** D for confined events (mean ± SEM for trajectories). **(h)** D for free-diffusive events (mean ± SEM for trajectories). β3-WT (6 cells, n=24861 trajectories), β3-N305T (5 cells, n=11083 trajectories), β3-D119Y (6 cells, n=17160 trajectories), β3-Y747A (5 cells, n=22260 trajectories) (also see Supplementary table S3). When indicated, statistical significances were obtained with a two-tailed Student's t-test comparing inside FAs, the different conditions vs. the β3-WT condition and outside FAs, comparing inside vs. outside values for each given condition. Otherwise, a black line indicates which pair of conditions was compared.

Figure S3. Measurements of immobilization zones duration using sptPALM

(a) High resolution image of β3-WT density (middle) in a FA (left: labeled with GFP-VASP) obtained from sptPALM sequence (duration: 400s) showing zones of β3-WT immobilization, scale bar, 2 μm. Boxed area, region shown at right, scale bar, 500 nm. **(b)** Fluorescence intensity versus time from the circled immobilization zone in **a** showing repetitive mEOS2 single fluorescent events (raw data). Short single fluorescent events (less than 3 points) that might correspond to trajectories only crossing the immobilization zone, were filtered out per our analysis method (filtered data). Longer single fluorescent events were used to determine the lifetimes. Lifetime (36 s) was measured as the time interval between the first and the last mEOS2 detection at the immobilization zone (see methods).

Figure S4. 6His-β3-integrins were efficiently labeled with TrisNTA-ATTO647N.

(a) Schematic of the labeling by TrisNTA-ATTO647N of 6His-β3-WT used during SMT experiments. **(b)** Labeling of 6His-β3-WT by TrisNTA-ATTO647N (middle) showed strong co-localization with FAs detected by GFP-VASP (left) in MEFs, scale bar, 5 μm. **(c-e)** Same labeling strategy used for respectively 6His-β3-N305T, 6His-β3-D119Y, 6His-β3-Y747A.

Figure S5. ABP binding induces β3-integrin immobilization more than FN.

(a) SMT experiments of 6His-β3-WT in MEFs using TrisNTA-ATTO647N labeling strategy. Trajectories overlaid on the FAs image (gray scale). Displacement between consecutive time points (STEP) are color-coded (LOG($STEP^2$)), from red (confined diffusion) to blue (free diffusion). Boxed area (left), region shown in the middle, scale bar, 1 μm. Variation of $STEP^2$

as function of time (right). **(b-d)** Same for respectively 6His-β3-N305T, 6His-β3-D119Y, 6His-β3-Y747A. Distribution of $STEP^2$ (logarithmic scale, base 10) inside **(e)** and outside **(f)** FAs. Both inside and outside FAs, we found two populations: one including immobile and slowly mobile molecules, and the other displaying faster mobility. The fractions of these two populations **(g)**, for all conditions, were in agreement with the fraction of immobilization measured by sptPALM. 6His-β3-WT (5 cells, 130 (517 after FA segmentation) trajectories), 6His-β3-WT + Mn^{2+} (16 cells, 194 (833 after FA segmentation) trajectories), 6His-β3-N305T (9 cells, 183 (484 after FA segmentation) trajectories), 6His-β3-D119Y (10 cells, 328 (1598 after FA segmentation) trajectories), 6His-β3-Y747A (6 cells, 301 (1643 after FA segmentation) trajectories), TM (7 cells, 244 (1010 after FA segmentation) trajectories).

Figure S6. Motion parameters for β3-WT, β1-WT, β1-D130Y, β1-Y783A, β3ext-β1int, β1ext-β3int

Motion parameters extracted from sptPALM experiments. **(a)** Distribution of LOG(D) inside and outside FAs (mean for cells) for β3-WT (black), β1-WT (brown), β3ext-β1int (dashed black) and β1ext-β3int (dashed brown). The gray areas including D values inferior to 0.008 $\mu m^2.s^{-1}$ correspond to immobile trajectories. **(b)** D for confined events (mean ± SEM for trajectories) inside and outside FAs for β3-WT (black), β1-WT (brown), β1-D130Y (green) and β1-Y783A (red) but also for the chimeras β3ext-β1int (black) and β1ext-β3int (brown). **(c)** D for free-diffusive events (mean ± SEM for trajectories). β3-WT (9 cells, n=23804 trajectories), β1-WT (9 cells, 21749 trajectories), β1-D130Y (10 cells, 13593 trajectories), β1-Y783A (7 cells, 7665 trajectories), β3ext-β1int (8 cells, 10756 trajectories), β1ext-β3int (6 cells, 8848 trajectories) (also see Supplementary table S1). **(d)** Cumulative distribution of immobilization duration measured from sptPALM, inside (left) and outside (right) FAs for β3-WT (black, 9 cells, 10821 immobilization events), β1-WT (brown, 6 cells, 5513 immobilization events), β1-D130Y (green, 6 cells, 1963 immobilization events), β1-Y783A (red, 5 cells, 995 immobilization events). When indicated, statistical significances were obtained with a two-tailed Student's t-test comparing inside FAs, the different conditions vs. the β1-WT condition and outside FAs, comparing inside vs. outside values for each given condition. Otherwise, a black line indicates which pair of conditions was compared.

Figure S7. STED imaging confirms the differential nano-scale organization of β3- and β1-integrins in FAs

(a) STED super-resolved image of transfected human β3-integrin-GFP labelled with a monoclonal anti human integrin αvBeta3 (clone LM609) and detected by ATTO647N labeled secondary antibody. Confocal image of β3-integrin-GFP (upper left), β3-integrin STED image (upper middle), merged image (upper right), scale bars, 5 μm. Boxed areas, regions shown at the bottom, scale bars, 1 μm. **(b)** STED super-resolved image of endogenous mouse β1-integrin labelled with a monoclonal antibody (clone 9EG7) and detected by ATTO647N labeled secondary antibody. Confocal image of β3-integrin-GFP (upper left), β1-integrin STED image (upper middle), merged image (upper right), scale bars, 5 μm. Boxed areas, regions shown on the bottom, scale bars, 1 μm.

Supplementary Tables and legends:

Table S1: sptPALM, MEFs co-transfected with GFP-paxillin

	β3-WT-mEOS2		**β3-N305T-mEOS2**		**β3-WT-mEOS2+Mn^{2+}**	
trajectories, cells	23804, 9		8876, 7		12910, 4	
	%	$Dx10^3$ ($\mu m^2/s$)	%	$Dx10^3$ ($\mu m^2/s$)	%	$Dx10^3$ ($\mu m^2/s$)
immobile FA	69 ± 2	<8	81 ± 2	<8	74 ± 2	<8
confined FA	14 ± 1	43 ± 1	11 ± 1	27 ± 2	13 ± 1	26 ± 1
free-diffusive FA	17 ± 1	76 ± 1	8 ± 1	46 ± 3	13 ± 1	43 ± 1
Immobile OUT	46 ± 3	<8	84 ± 5	<8	86 ± 3	<8
confined OUT	15 ± 1	189 ± 5	9 ± 3	61 ± 4	6 ± 2	43 ± 3
free-diffusive OUT	39 ± 3	289 ± 3	7 ± 3	130 ± 7	8 ± 2	109 ± 5
r_{conf} FA (nm), 0.4s	119 ± 1		100 ± 2		103 ± 1	
r_{conf} OUT (nm), 0.4s	236 ± 3		133 ± 4		118 ± 3	
	β3-D119Y-mEOS2		**β3-Y747A-mEOS2**		**TM-mEOS2**	
trajectories, cells	23784, 6		17894, 6		14256, 5	
	%	$Dx10^3$ ($\mu m^2/s$)	%	$Dx10^3$ ($\mu m^2/s$)	%	$Dx10^3$ ($\mu m^2/s$)
immobile FA	49 ± 3	<8	41 ± 4	<8	31 ± 5	<8
confined FA	19 ± 2	76 ± 2	21 ± 1	106 ± 5	19 ± 1	135 ± 6
free-diffusive FA	32 ± 2	123 ± 3	38 ± 3	148 ± 4	50 ± 3	172 ± 4
Immobile OUT	15 ± 2	<8	18 ± 2	<8	22 ± 5	<8
confined OUT	21 ± 1	261 ± 3	21 ± 5	229 ± 4	20 ± 1	201 ± 5
free-diffusive OUT	64 ± 2	354 ± 2	61 ± 2	326 ± 2	58 ± 4	280 ± 3
r_{conf} FA (nm), 0.4s	154 ± 2		178 ± 4		203 ± 4	
r_{conf} OUT (nm), 0.4s	286 ± 2		268 ± 2		246 ± 3	
	CAAX-mEOS2					
trajectories, cells	8008, 6					
	%	$Dx10^3$ ($\mu m^2/s$)				
immobile FA	29 ± 4	<8				
confined FA	23 ± 1	368 ± 1				
free-diffusive FA	48 ± 3	482 ± 10				
Immobile OUT	34 ± 3	<8				
confined OUT	21 ± 1	377 ± 11				
free-diffusive OUT	45 ± 2	578 ± 9				
r_{conf} FA (nm), 0.4s	326 ± 7					
r_{conf} OUT (nm), 0.4s	318 ± 6					

	β1-WT-mEOS2		**β1-D130Y-mEOS2**		**β1-Y783A-mEOS2**	
trajectories, cells	21749, 9		13593, 10		7665, 7	
	%	$Dx10^3$ ($\mu m^2/s$)	%	$Dx10^3$ ($\mu m^2/s$)	%	$Dx10^3$ ($\mu m^2/s$)
immobile FA	79 ± 2	<8	80 ± 2	<8	45 ± 4	<8
confined FA	11 ± 1	49 ± 3	10 ± 1	36 ± 2	23 ± 3	99 ± 7
free-diffusive FA	10 ± 1	89 ± 4	10 ± 1	70 ± 3	32 ± 3	153 ± 7
Immobile OUT	46 ± 6	<8	57 ± 5	<8	31 ± 4	<8
confined OUT	17 ± 1	200 ± 4	17 ± 1	120 ± 5	23 ± 1	219 ± 5
free-diffusive OUT	37 ± 5	299 ± 3	26 ± 4	220 ± 4	46 ± 4	322 ± 4
r_{conf} FA (nm), 0.4s	124 ± 2		115 ± 2		175 ± 6	
r_{conf} OUT (nm), 0.4s	241 ± 3		187 ± 3		261 ± 4	
	β1ext-β3int-mEOS2		**β3ext-β1int-mEOS2**			
trajectories, cells	8848, 6		10756, 8			
	%	$Dx10^3$ ($\mu m^2/s$)	%	$Dx10^3$ ($\mu m^2/s$)		
immobile FA	79 ± 1	<8	70 ± 2	<8		
confined FA	14 ± 1	36 ± 3	16 ± 1	33 ± 1		
free-diffusive FA	7 ± 1	78 ± 5	14 ± 2	68 ± 3		
Immobile OUT	59 ± 3	<8	54 ± 7	<8		
confined OUT	17 ± 1	122 ± 5	17 ± 1	154 ± 7		
free-diffusive OUT	24 ± 2	233 ± 5	29 ± 5	277 ± 6		
r_{conf} FA (nm), 0.4s	120 ± 2		120 ± 2			
r_{conf} OUT (nm), 0.4s	192 ± 4		208 ± 5			

Values correspond to mean ± SEM

β3-WT: 9 cells; immobile inside/outsie FAs n=10672/3777 trajectories; confined inside/outsie FAs n=2204/1280 trajectories; free-diffusive inside/outside FAs n=2636/3235 trajectories. **β3-N305T:** 7 cells; immobile inside/outsie FAs n=3018/4394 trajectories; confined inside/outsie FAs n=407/424 trajectories; free-diffusive inside/outside FAs n=294/339 trajectories. **β3-WT + Mn^{2+}:** 4 cells; immobile inside/outsie FAs n=5229/5037 trajectories; confined inside/outsie FAs n=966/330 trajectories; free-diffusive inside/outside FAs n=932/416 trajectories. **β3-D119Y:** 6 cells; immobile inside/outsie FAs n=3274/2610 trajectories; confined inside/outsie FAs n=1399/3638 trajectories; free-diffusive inside/outside FAs n=2274/10589 trajectories. **β3-Y747A:** 6 cells; immobile inside/outsie FAs n=1324/2695 trajectories; confined inside/outsie FAs n=699/3086 trajectories; free-diffusive inside/outside FAs n=1251/8839 trajectories. **TM:** 5 cells; immobile inside/outsie FAs n=618/2091 trajectories; confined inside/outsie FAs n=618/2091 trajectories; free-diffusive inside/outside FAs n=1610/6012 trajectories. **CAAX** 6 cells; immobile inside/outsie FAs n=658/1992 trajectories; confined inside/outsie FAs n=561/1159 trajectories; free-diffusive inside/outside FAs n=1160/2478 trajectories. **β1-WT:** 9 cells; immobile inside/outsie FAs n=7162/5892 trajectories; confined inside/outsie FAs n=952/2082 trajectories; free-diffusive inside/outside

FAs n=922/4739 trajectories. **β1-D130Y:** 10 cells; immobile inside/outsie FAs n=5275/4053 trajectories; confined inside/outsie FAs n=736/1104 trajectories; free-diffusive inside/outside FAs n=684/1741 trajectories. **β1-Y783A:** 7 cells; immobile inside/outsie FAs n=631/1762 trajectories; confined inside/outsie FAs n=291/1412 trajectories; free-diffusive inside/outside FAs n=457/3112 trajectories. **β1extβ3int:** 6 cells; immobile inside/outsie FAs n=2802/3145 trajectories; confined inside/outsie FAs n=496/886 trajectories; free-diffusive inside/outside FAs n=278/1232 trajectories. **β3extβ1int:** 8 cells; immobile inside/outsie FAs n=4074/2689 trajectories; confined inside/outsie FAs n=931/816 trajectories; free-diffusive inside/outside FAs n=878/1368 trajectories.

Table S2: sptPALM, MEFs co-transfected with GFP-VASP

	β3-WT-mEOS2		**β3-N305T-mEOS2**		**β3-WT-mEOS2+Mn^{2+}**	
trajectories, cells	15798, 10		3510, 4		13591, 5	
	%	$Dx10^3$ ($\mu m^2/s$)	%	$Dx10^3$ ($\mu m^2/s$)	%	$Dx10^3$ ($\mu m^2/s$)
immobile FA	76 ± 4	<8	91 ± 1	<8	80 ± 2	<8
confined FA	12 ± 2	38 ± 2	6 ± 1	28 ± 3	13 ± 2	26 ± 1
free-diffusive FA	12 ± 2	74 ± 2	3 ± 1	70 ± 1	7 ± 2	40 ± 2
Immobile OUT	53 ± 4	<8	84 ± 4	<8	83 ± 5	<8
confined OUT	14 ± 1	189 ± 5	9 ± 2	42 ± 5	10 ± 4	45 ± 4
free-diffusive OUT	33 ± 3	279 ± 4	7 ± 3	129 ± 9	7 ± 1	117 ± 6
r_{conf} FA (nm), 0.4s	118 ± 2		103 ± 4		104 ± 1	
r_{conf} OUT (nm), 0.4s	236 ± 4		121 ± 5		119 ± 3	
	β3-D119Y-mEOS2		**β3-Y747A-mEOS2**		**TM-mEOS2**	
trajectories, cells	20130, 8		17089, 5		11431, 11	
	%	$Dx10^3$ ($\mu m^2/s$)	%	$Dx10^3$ ($\mu m^2/s$)	%	$Dx10^3$ ($\mu m^2/s$)
immobile FA	52 ± 4	<8	38 ± 3	<8	28 ± 6	<8
confined FA	18 ± 1	86 ± 3	21 ± 1	104 ± 3	21 ± 2	177 ± 7
free-diffusive FA	30 ± 3	138 ± 3	41 ± 3	149 ± 3	51 ± 5	229 ± 5
Immobile OUT	37 ± 5	<8	33 ± 4	<8	32 ± 6	<8
confined OUT	19 ± 1	242 ± 5	20 ± 1	223 ± 4	19 ± 1	255 ± 5
free-diffusive OUT	44 ± 4	365 ± 3	47 ± 4	328 ± 3	49 ± 5	357 ± 3
r_{conf} FA (nm), 0.4s	166 ± 2		184 ± 2		236 ± 5	
r_{conf} OUT (nm), 0.4s	267 ± 3		259 ± 3		281 ± 3	
	CAAX-mEOS2		**β1-WT-mEOS2**			
trajectories, cells	9145, 8		35235, 16			
	%	$Dx10^3$ ($\mu m^2/s$)	%	$Dx10^3$ ($\mu m^2/s$)		
immobile FA	29 ± 4	<8	73 ± 1	<8		
confined FA	27 ± 1	320 ± 15	12 ± 1	56 ± 2		
free-diffusive FA	44 ± 3	452 ± 11	15 ± 1	108 ± 3		
Immobile OUT	39 ± 2	<8	43 ± 5	<8		
confined OUT	21 ± 1	319 ± 10	16 ± 1	187 ± 3		
free-diffusive OUT	40 ± 2	574 ± 9	41 ± 4	272 ± 2		
r_{conf} FA (nm), 0.4s	294 ± 7		133 ± 2			
r_{conf} OUT (nm), 0.4s	289 ± 5		238 ± 2			

Values correspond to mean ± SEM

β3-WT: 10 cells; immobile inside/outsie FAs n=5602/3981 trajectories; confined inside/outsie FAs n=1119/1128 trajectories; free-diffusive inside/outside FAs n=1152/2816

trajectories. **β3-N305T:** 4 cells; immobile inside/outsie FAs n=1333/1731 trajectories; confined inside/outsie FAs n=95/175 trajectories; free-diffusive inside/outside FAs n=47/129 trajectories. **β3-WT + Mn^{2+}:** 5 cells; immobile inside/outsie FAs n=4862/6487 trajectories; confined inside/outsie FAs n=721/471 trajectories; free-diffusive inside/outside FAs n=568/482 trajectories. **β3-D119Y:** 8 cells; immobile inside/outsie FAs n=3403/4040 trajectories; confined inside/outsie FAs n=1412/2495 trajectories; free-diffusive inside/outside FAs n=2482/6301 trajectories. **β3-Y747A:** 5 cells; immobile inside/outsie FAs n=2079/3519 trajectories; confined inside/outsie FAs n=1273/2302 trajectories; free-diffusive inside/outside FAs n=2343/5573 trajectories. **TM:** 11 cells; immobile inside/outsie FAs n=422/2530 trajectories; confined inside/outsie FAs n=445/1903 trajectories; free-diffusive inside/outside FAs n=1074/5057 trajectories. **CAAX:** 8 cells; immobile inside/outsie FAs n=822/2714 trajectories; confined inside/outsie FAs n=532/1509 trajectories; free-diffusive inside/outside FAs n=963/2605 trajectories. **β1-WT:** 16 cells; immobile inside/outsie FAs n=8122/9793 trajectories; confined inside/outsie FAs n=1334/3981 trajectories; free-diffusive inside/outside FAs n=1566/10439 trajectories.

Table S3: sptPALM, β3-integrin $^{-/-}$ MEFs co-transfected with GFP-paxillin

	β3-WT-mEOS2		**β3-N305T-mEOS2**		**β3-D119Y-mEOS2**	
trajectories, cells	24861, 6		11083, 5		17160, 6	
	%	Dx10^3 (μm^2/s)	%	Dx10^3 (μm^2/s)	%	Dx10^3 (μm^2/s)
immobile FA	73 ± 2	<8	84 ± 3	<8	52 ± 3	<8
confined FA	13 ± 1	38 ± 1	11 ± 3	23 ± 1	19 ± 2	57 ± 2
free-diffusive FA	14 ± 1	72 ± 2	5 ± 1	37 ± 4	29 ± 3	90 ± 2
Immobile OUT	48 ± 7	<8	86 ± 2	<8	38 ± 4	<8
confined OUT	16 ± 1	174 ± 4	10 ± 2	29 ± 2	20 ± 1	139 ± 3
free-diffusive OUT	36 ± 6	274 ± 3	4 ± 1	78 ± 5	42 ± 4	215 ± 2
r_{conf} FA (nm), 0.4s	118 ± 1		101 ± 2		140 ± 2	
r_{conf} OUT (nm), 0.4s	226 ± 3		104 ± 2		210 ± 2	
	β3-Y747A-mEOS2					
trajectories, cells	22260, 5					
	%	Dx10^3 (μm^2/s)				
immobile FA	38 ± 4	<8				
confined FA	23 ± 1	80 ± 3				
free-diffusive FA	39 ± 3	113 ± 3				
Immobile OUT	24 ± 4	<8				
confined OUT	22 ± 1	163 ± 2				
free-diffusive OUT	54 ± 4	240 ± 2				
r_{conf} FA (nm), 0.4s	154 ± 2					
r_{conf} OUT (nm), 0.4s	286 ± 2					

Values correspond to mean ± SEM

β3-WT: 6 cells; immobile inside/outsie FAs n=9757/5171 trajectories; confined inside/outsie FAs n=1866/1814 trajectories; free-diffusive inside/outside FAs n=1918/4335 trajectories. **β3-N305T:** 5 cells; immobile inside/outsie FAs n=2807/6571 trajectories; confined inside/outsie FAs n=396/788 trajectories; free-diffusive inside/outside FAs n=163/358 trajectories. **β3-D119Y:** 6 cells; immobile inside/outsie FAs n=3547/3893 trajectories; confined inside/outsie FAs n=1302/2158 trajectories; free-diffusive inside/outside FAs n=1833/4427 trajectories. **β3-Y747A:** 5 cells; immobile inside/outsie FAs n=1975/4293 trajectories; confined inside/outsie FAs n=1080/3750 trajectories; free-diffusive inside/outside FAs n=1799/9363 trajectories.

Supplementary Movie Legends

Movie S1. 6His-β3-WT switches between free-diffusion and immobilization states when entering a FA

This movie shows the time course of the SMT experiment depicted in Fig. 3d and Supplementary Fig. S5a. It covers a period of about 23 seconds, during which a single ATTO647N (red) labeling one 6His-β3-WT is tracked and displayed transitions from fast free-diffusion outside FA (1), to slow free-diffusion (2) and immobilization (3) when entering a FA (in green). Scale bar = 1.5 μm. Speed, 8X. (Avi; 886 KB)

Figure S1-Giannone

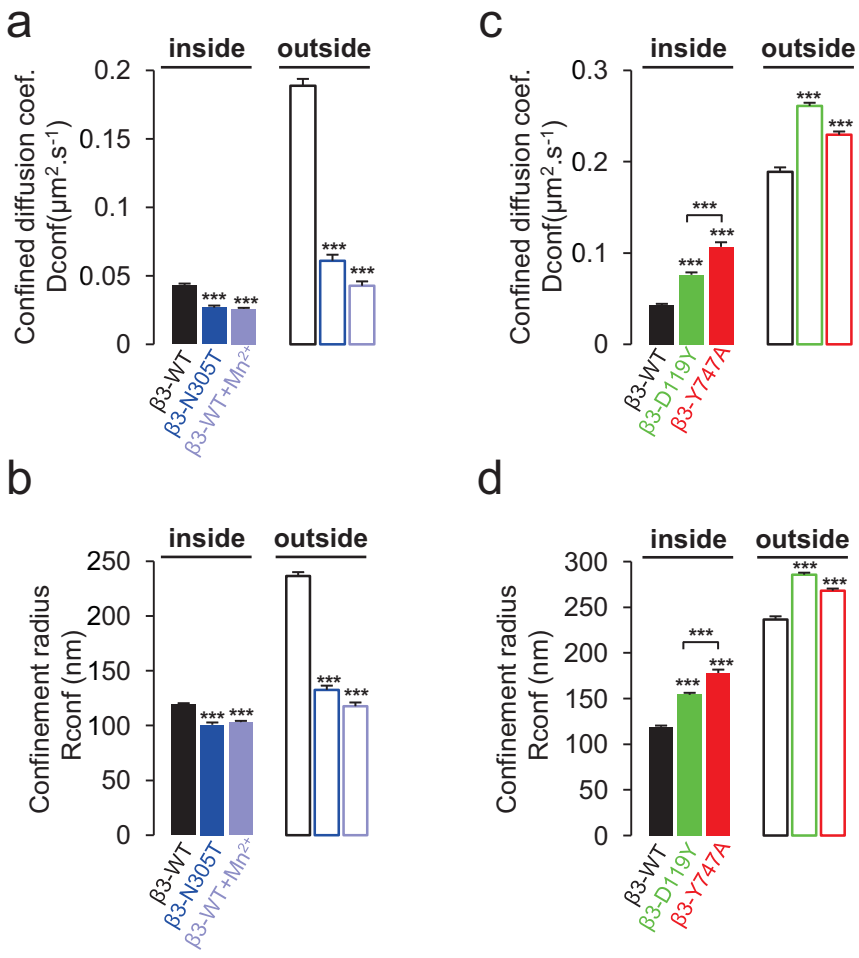

Figure S2-Giannone

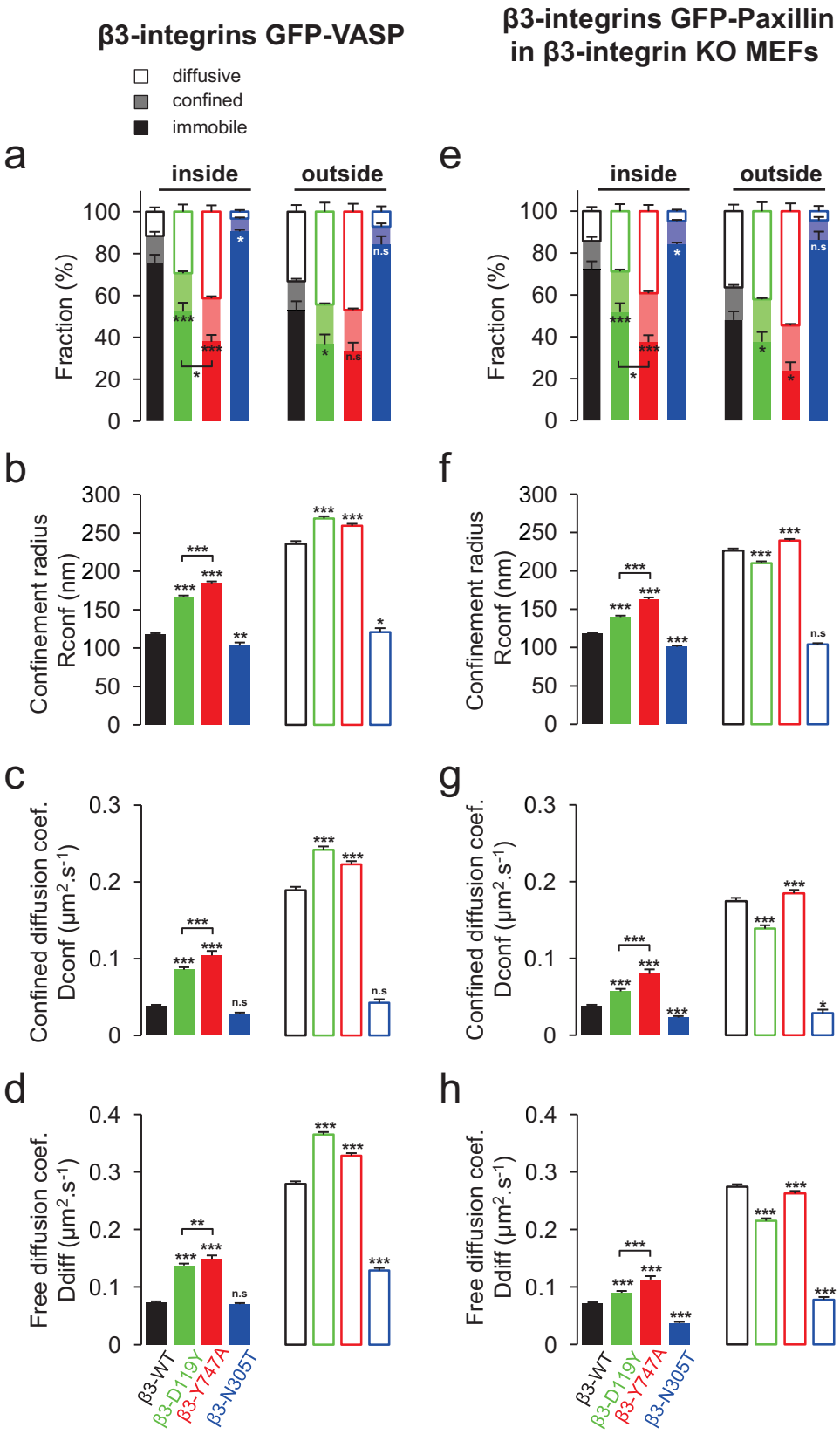

Figure S3-Giannone

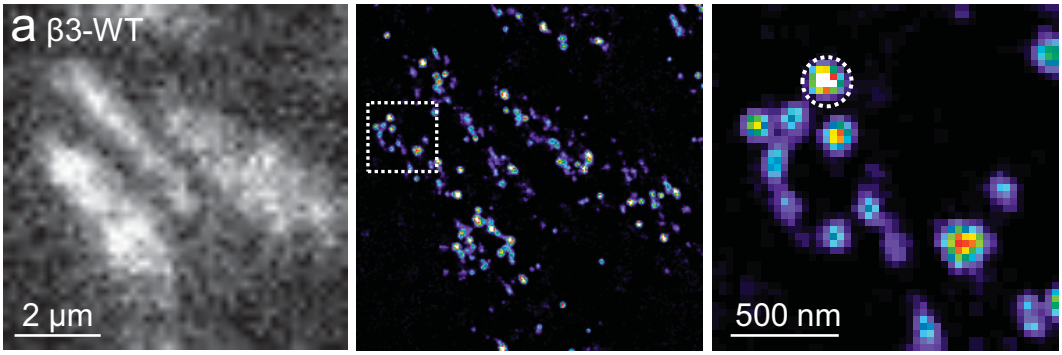

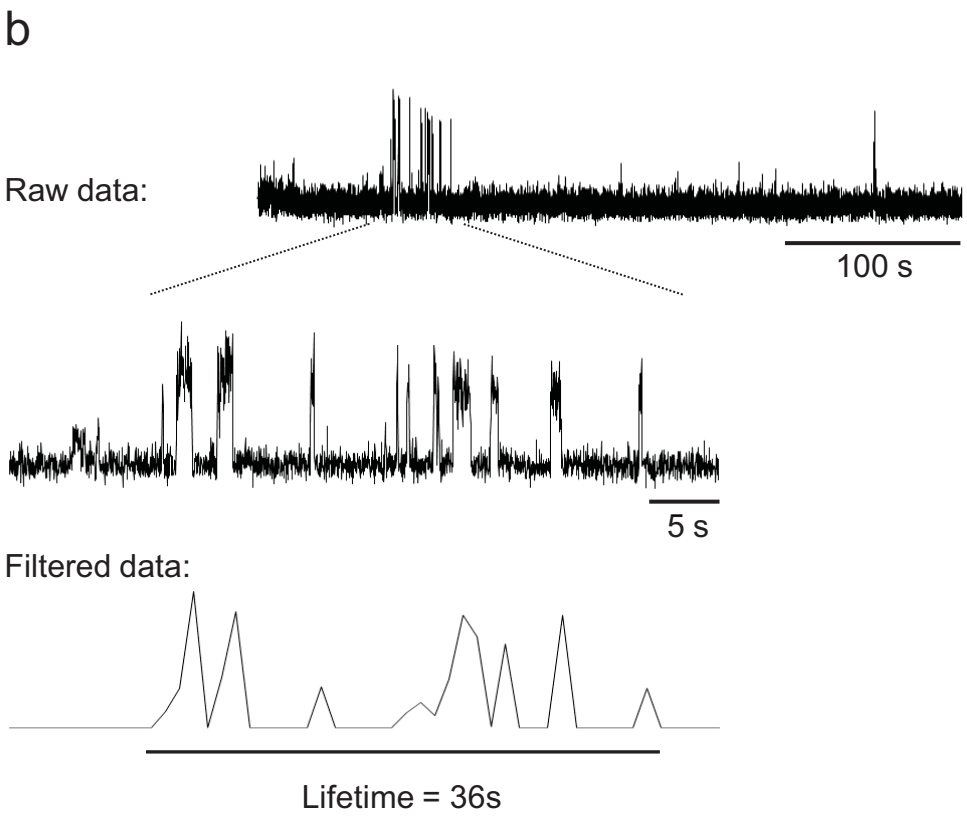

Figure S4-Giannone

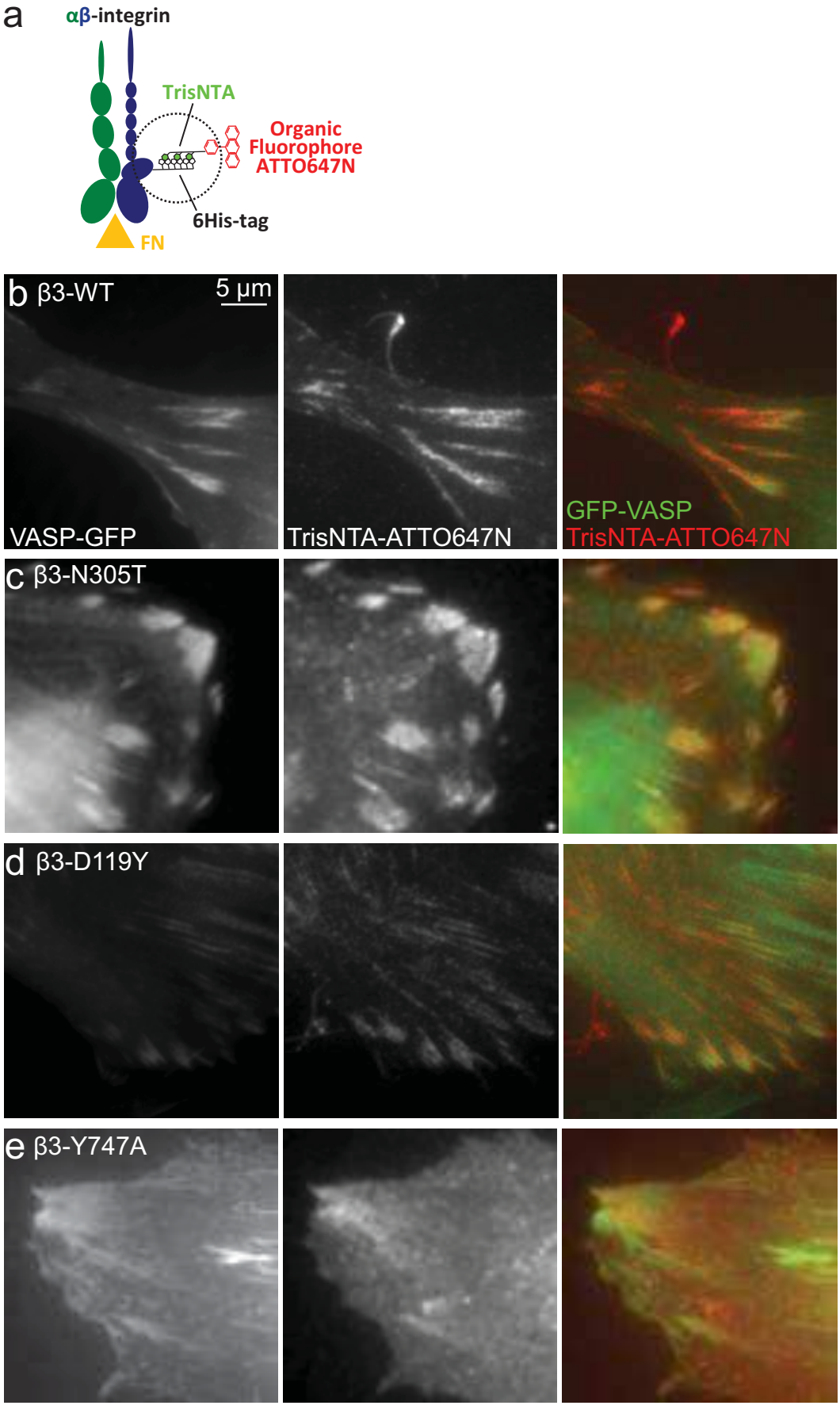

Figure S5-Giannone

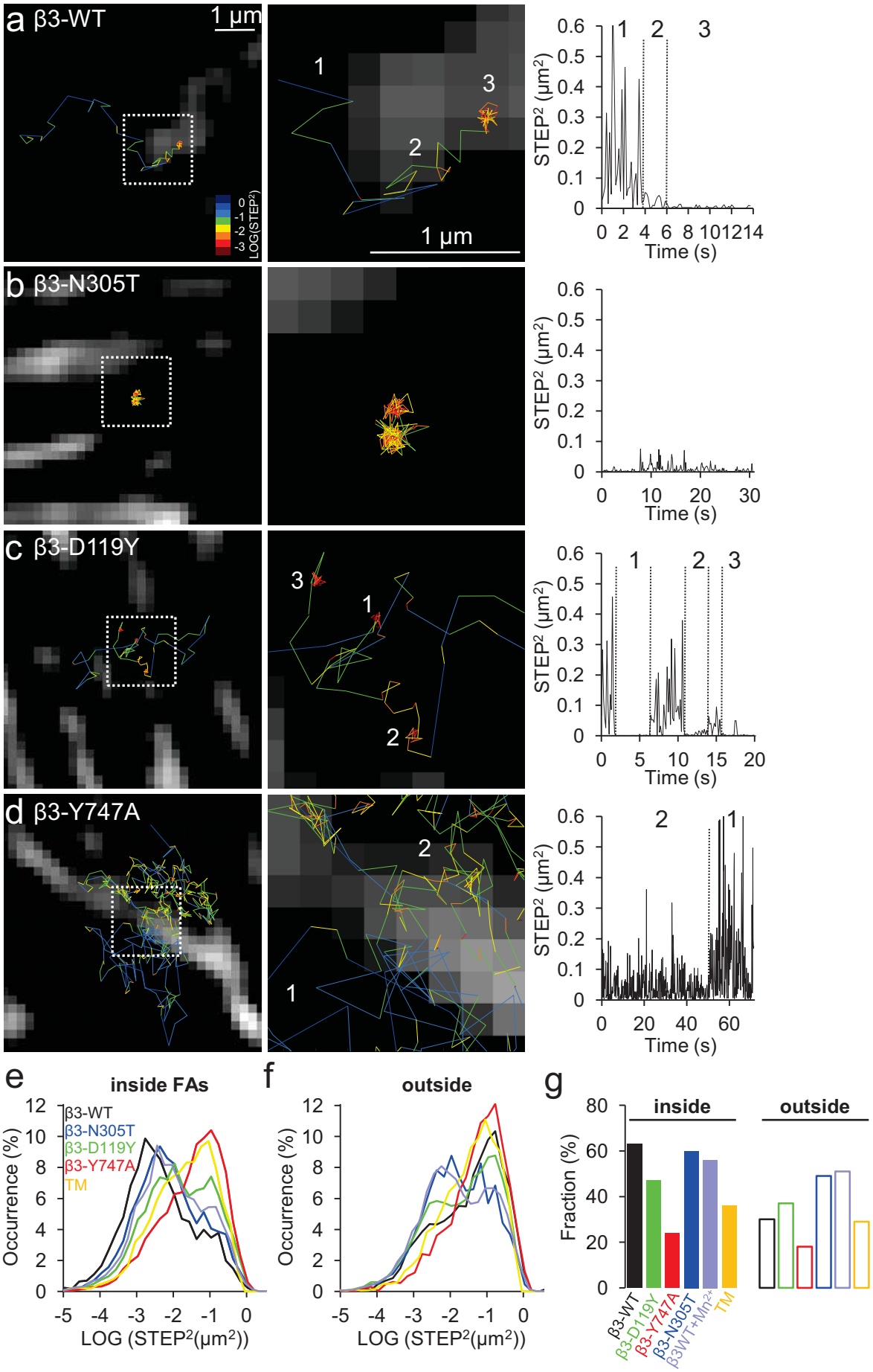

Figure S6-Giannone

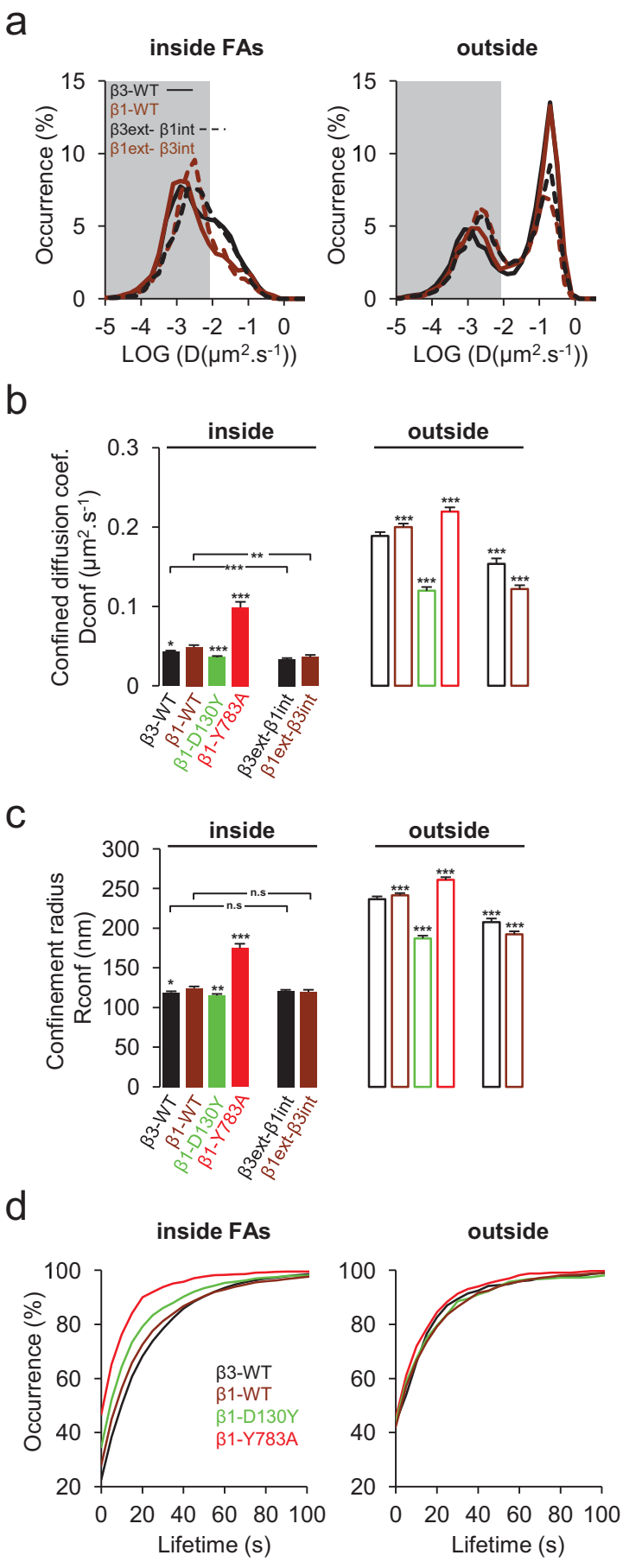

Figure S7-Giannone